General OCR Theory: Towards OCR-2.0 via a Unified End-to-end Model

Haoran Wei[1,*], **Chenglong Liu**[3,*], **Jinyue Chen**[3], **Jia Wang**[1], **Lingyu Kong**[3], **Yanming Xu**[1], **Zheng Ge**[1], **Liang Zhao**[1], **Jianjian Sun**[1], **Yuang Peng**[4], **Chunrui Han**[2], **Xiangyu Zhang**[1,2]

[1]StepFun [2]Megvii Technology
[3]University of Chinese Academy of Sciences [4]Tsinghua University
https://github.com/Ucas-HaoranWei/GOT-OCR2.0

Abstract

Traditional OCR systems (OCR-1.0) are increasingly unable to meet people's usage due to the growing demand for intelligent processing of man-made optical characters. In this paper, we collectively refer to all artificial optical signals (e.g., plain texts, math/molecular formulas, tables, charts, sheet music, and even geometric shapes) as "characters" and propose the **G**eneral **O**CR **T**heory along with an excellent model, namely GOT, to promote the arrival of OCR-2.0. The GOT, with 580M parameters, is a unified, elegant, and end-to-end model, consisting of a high-compression encoder and a long-contexts decoder. As an OCR-2.0 model, GOT can handle all the above "characters" under various OCR tasks. On the input side, the model supports commonly used scene- and document-style images in slice and whole-page styles. On the output side, GOT can generate plain or formatted results (markdown/tikz/smiles/kern) via an easy prompt. Besides, the model enjoys interactive OCR features, i.e., region-level recognition guided by coordinates or colors. Furthermore, we also adapt dynamic resolution and multi-page OCR technologies to GOT for better practicality. In experiments, we provide sufficient results to prove the superiority of our model.

1 Introduction

Optical Character Recognition (OCR) is a widely used technology that extracts the characters embedded in an optical image into an editable format. Typical OCR systems [10] in the OCR-1.0 era are mainly designed based on a multi-modular pipeline style, commonly including element detection, region cropping, and character recognition parts. Each module is prone to falling into local optima, making the whole system incur high maintenance costs. Moreover, traditional OCR methods have insufficient general ability, reflected as different OCR-1.0 networks usually designed for different sub-tasks. Nevertheless, choosing a suitable one from diverse OCR models for a special task is always inconvenient for users.

In the past year, Large Vision Language models (LVLMs) [5, 9, 24, 27, 36, 46, 49] have developed rapidly and showcased impressive performance. As a highly anticipated ability, the OCR performance of current LVLMs is continuously improving. Based on CLIP [37], LLaVA [24] naturally acquires the English OCR ability after the instruct tuning phase. To lift the OCR accuracy and support other languages, e.g., Chinese, Qwen-VL [5] unfreezes its image encoder (a CLIP-G) and uses lots of OCR data in its stage-two training. Innovatively, Vary [46] generates a new high-resolution OCR vision vocabulary paralleling the CLIP branch to deal with document-level dense OCR. By contrast,

[*] Equal contribution

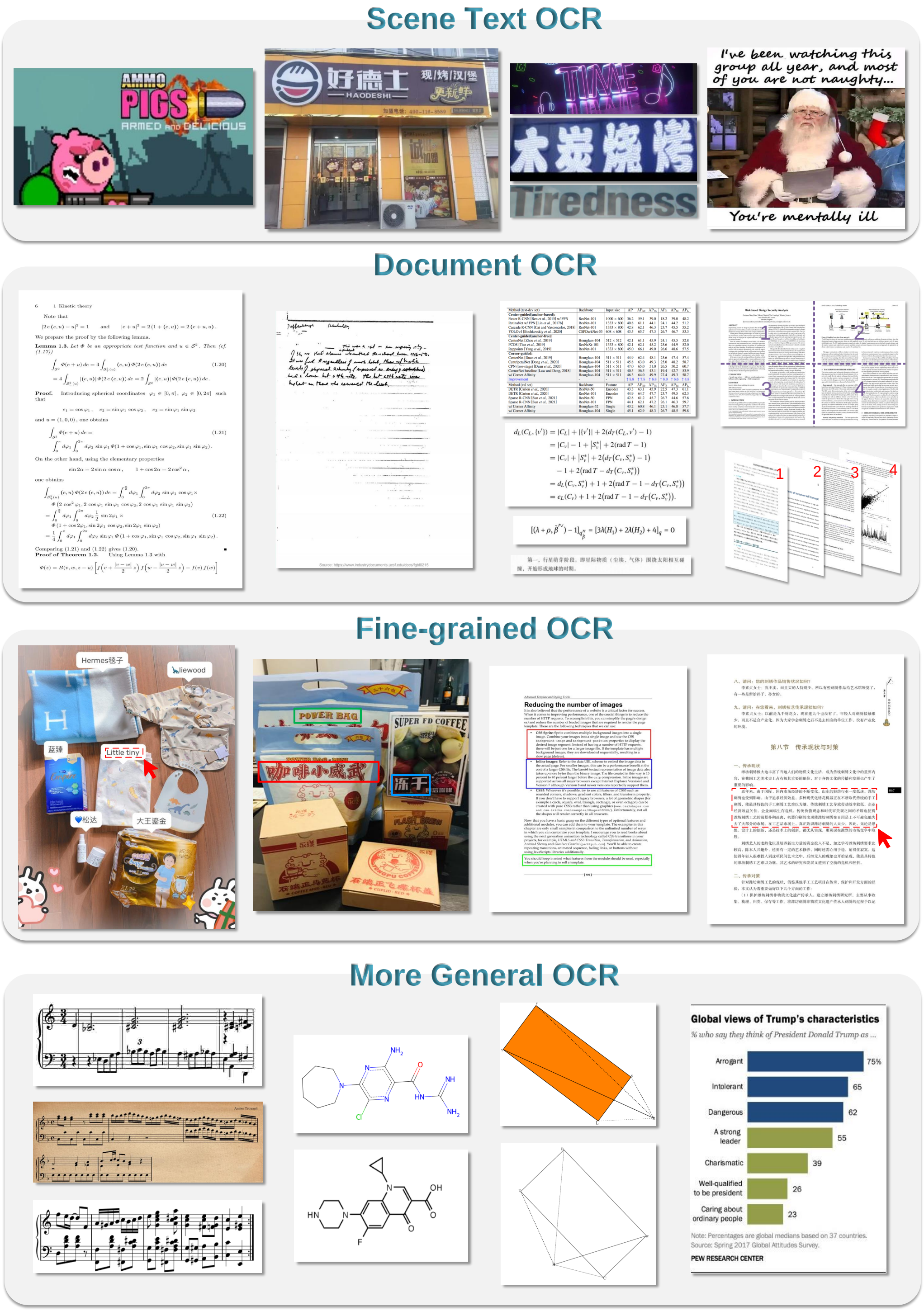
Scene Text OCR
AMMO PIGS
ARMED AND DELICIOUS
好德士
HAODESHI
现/烤/汉/堡
TIME
木炭烧烤
Tiredness
I've been watching this group all year, and most of you are not naughty...
You're mentally ill
Document OCR
1
2
3
4
Fine-grained OCR
Hermes毯子
liewood
蓝臻
Little tiny
松达
大王童全
POWER BAG
咖啡小威武
SUPER FD COFFEE
冻干
Reducing the number of images
第八节 传承现状与对策
More General OCR
NH2
N
Cl
HN
NH
OH
F
O
Global views of Trump's characteristics
% who say they think of President Donald Trump as ...
Arrogant 75%
Intolerant 65
Dangerous 62
A strong leader 55
Charismatic 39
Well-qualified to be president 26
Caring about ordinary people 23
Note: Percentages are global medians based on 37 countries.
Source: Spring 2017 Global Attitudes Survey.
PEW RESEARCH CENTER

Figure 1: On the input side, GOT supports various optical image types, such as commonly used photographs and documents. Besides, as a general OCR-2.0 model, GOT can handle more tasks, e.g., sheet music, molecular formulas, easy geometric shapes, charts, etc. Moreover, the model can adapt to region-focus OCR, high-resolution OCR, and multiple-page OCR. GOT mainly supports English and Chinese and can control the structure results (Mathpix markdown/tikz/smiles/kern) via a prompt.

InternVL-1.5 [9] and other models [27, 50] utilize a sliding window manner to crop the whole image into multiple sub-patches for high-resolution OCR. Hence, a consensus is that optical character perception and recognition are the foundation of text-driven image understanding, drawing many researchers to pay more attention to LVLMs' OCR booster.

However, the popular designs of LVLMs may not be suitable for diverse OCR tasks for the following reasons: 1) The conflicts between perception and reasoning. LVLMs mainly focus on visual reasoning performance, e.g., VQA [33, 42], because that is what the LLM excels at. To quickly obtain the QA-gain benefits from LLMs, most LVLMs [15, 24, 49] align image tokens to text ones. However, it is unreasonable to do this for pure perception OCR tasks, especially high-density text scenes, because each aligned vision token (biased towards text token) cannot compress enough characters. Imagine how wasteful it is to use thousands of image tokens, e.g., the image-cropping manner [9, 23], to encode an equal amount of optical characters (e.g., texts within only an A4-PDF page). 2) High iteration and deployment costs. LVLM often enjoys billions of parameters, leading to the post-training and deployment costs being too high. Generally speaking, for LVLMs, fine-tuning is not enough once we want to add a new OCR pattern, e.g., a new language, instead of enough GPU resources for pre-training. However, rerunning the pre-training with billions of parameters, only to introduce a new OCR feature, is also wasteful.

Accordingly, we propose the general OCR theory, i.e., OCR-2.0, to break the bottlenecks of both traditional and LVLM manners on OCR tasks. We think that a model of OCR 2.0 should have the following essential characteristics:

- **End-to-end.** Compared to OCR-1.0 models with complex procedures, the OCR-2.0 model should enjoy a unified and end-to-end architecture to ensure lower maintenance costs. It is cool that a beginner can quickly master the entire OCR system in the 2.0 era.

- **Low training and inference costs.** The OCR-2.0 model should not be a chatbot, like LVLM, that focuses on reasoning tasks. Its focus should be on strong perception and recognition of optical characters, so it needs a reasonable number of model parameters in exchange for lower training and inference costs.

- **Versatility.** The OCR-2.0 model's other important point is versatility, including recognizing more general artificial optical "characters", e.g., sheet music, charts, geometric shapes, etc. Besides, the model should support the output format with stronger readability, e.g., LaTeX/Markdown format for formulas and tables.

Based on the proposed general OCR theory, we present a primary OCR-2.0 model (GOT) to bridge the gap between OCR-1.0 models and people's higher optical character processing demands. In architecture, we adopt the unsophisticated encoder-decoder paradigm for the model. Specifically, GOT enjoys a high compression rate encoder to transfer the optical image to tokens as well as a long context length decoder to output the corresponding OCR results. The encoder has approximately 80M parameters posing 1024×1024 input size which is enough to deal with commonly used photo/document input styles. Each input image will be compressed to tokens with 256×1024 dimensions. The decoder of GOT, with 0.5B parameters, supports 8K max length tokens to ensure it can tackle long-context scenarios. We devise an effective and efficient training strategy for GOT, which can be divided into three procedures, i.e., decoupled pre-training of the encoder, joint-training of the encoder with a new decoder, and further post-training of the decoder. Besides, to further lift the practicality of GOT, we additionally adapt the fine-grained OCR feature for better interactivity, dynamic resolution strategy for ultra-high-resolution images (e.g., over 2K), and the multi-page OCR technology to alleviate the problem of difficulty in breaking pages in PDF image-text pairs (e.g., page breaks in *.tex* files). To support each training stage, we do many data engines for synthetic data production, which is the key to the success of GOT and will be described in detail in this paper. The main input data format supported by our model can be seen in Figure 1.

As a model for envisioning OCR-2.0, GOT demonstrates promising performance in our experiments in various OCR tasks. We hope the proposed simple and elegant GOT can draw more researchers to invest in the research of OCR-2.0. Of course, the path to OCR-2.0 is still long and GOT also enjoys much improvement room, such as supporting more languages, more general artificial signals, and more complex geometries. In this new era led by LVLMs, we are convinced that the pure OCR model is not over, it may even be a new beginning.

2 Related Work

2.1 Traditional OCR

Optical Character Recognition (OCR) is a classic research topic that aims to convert the image's optical contents into an editable format for further downstream processing. Traditional OCR systems, called OCR-1.0, typically use a framework that is assembled from multiple expert modules. For instance, to handle diverse optical characters, the OCR system [10] is usually developed by integrating several domain expert networks, such as layout analysis [54], text detection [18, 19, 26, 30, 43, 45, 52, 55], region extraction, and contents recognition [11, 14, 16]. The reason for using such a pipeline scheme is that the text recognition module (the OCR part) failed to scale up successfully, which can only deal with the image format of small slices, resulting in the entire OCR process being in the form of first detecting texts/cropping regions, and then recognizing the results within the slice. However, a system with complicated procedures may suffer potential systematic errors and high maintenance costs. Although some OCR-1.0 models, e.g., Nougat [6] can directly process documents at the whole page level, they are often designed and trained for a specific sub-task, leading to unsatisfactory general ability. In the OCR-1.0 era, one inconvenient thing is that we usually need to switch different models according to various OCR needs.

2.2 LVLM-driven OCR

Large Vision-Language Models (LVLMs) [5, 9, 20, 24, 27, 46, 49] have attracted lots of attention in the AI-community due to their powerful generalization capabilities. For the current LVLMs owning perception-reasoning comprehensive capacity, the OCR ability has become a hot spot with the increasing demand for text-driven visual understanding. Most LVLMs' OCR capabilities come from the ready-made CLIP [37], especially those that freeze CLIP encoder [24] to complete the entire LVLM training. For such models, the vanilla CLIP, mainly with English scene text knowledge, is the bottleneck for the OCR performance to out-of-domain tasks, such as other languages or documents. Some other LVLMs [5, 49] choose to unfreeze the encoder and freeze the LLM for training to enhance the CLIP-encoder and align the image tokens to text ones. These models will face the problem of low optical character compression rate, as it is difficult for frozen LLM to decode too much text from an aligned image token. To alleviate this problem, some models [9, 27, 50] adopt a sliding window manner to decompose input images into smaller patches. Although this dynamic resolution approach is highly effective in processing high-resolution input images, e.g., PDF, it will result in excessive image tokens and limit the max length of the generated OCR result to some extent.

3 General OCR Theory

In this work, we propose the general OCR theory, i.e., OCR-2.0 (as expounded in Section 1) to promote the development of the OCR field. Based on the proposed new theory, we present a novel OCR model (GOT). In this section, we will introduce the technical details of our model, including the framework, multi-stage training strategy, and the corresponding data engines.

3.1 Framework

As illustrated in Figure 2, GOT comprises three modules, i.e., an image encoder, a linear layer, and an output decoder. The linear layer acts as the connector to map the channel dimension between the vision encoder and the language decoder. We utilize three main steps in optimizing the whole GOT model. First, we conduct the pure text recognition task to pre-train the vision encoder. To lift training efficiency and save GPU resources, we choose a tiny decoder to pass gradients to the encoder. In this stage, we feed images containing scene texts and manual images containing document-level characters into the model to allow the encoder to gather the two most commonly used characters' encoding abilities. In the next stage, we form the architecture of GOT by connecting the trained vision encoder to a new larger decoder. We prepare lots of more general OCR data (*e.g.*, sheet music, math/molecular formulas, and geometric shapes) to scale up the OCR-2.0 knowledge for this stage. In the final stage, we intend to improve the generalization and applicability of GOT further. Specifically, fine-grained and muti-crop/page synthetic data are generated and added for GOT to support region prompt OCR [20], huge image OCR, and batched PDF OCR features.

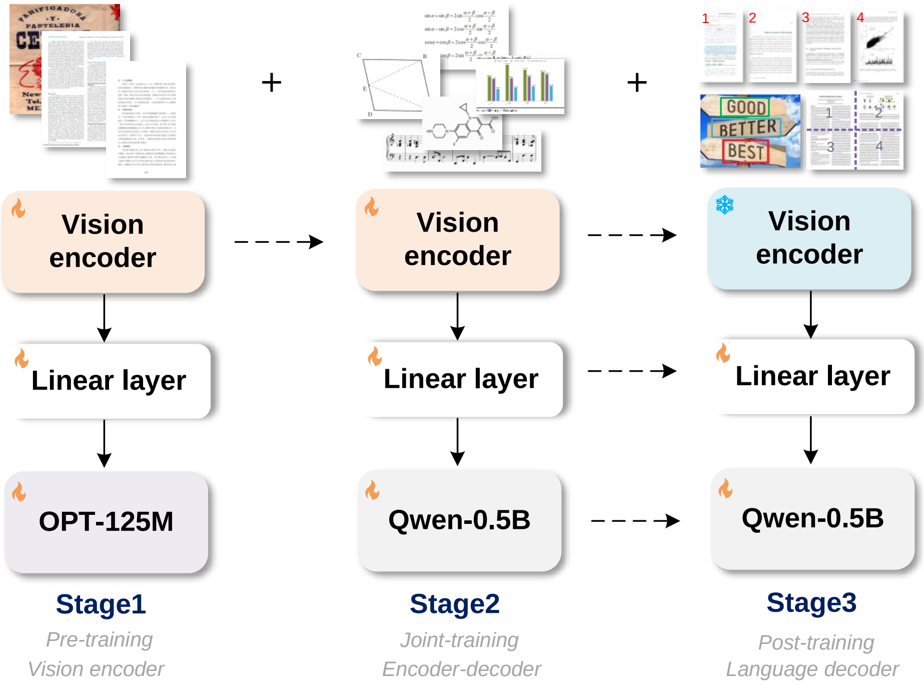

Figure 2: The framework of the proposed GOT. Stage 1: We pre-train the vision encoder using a tiny OPT-125M to adapt the OCR tasks efficiently. Stage 2: GOT is built by connecting the vision encoder to Qwen-0.5B and sufficient OCR-2.0 knowledge of more general optical characters is used in this stage. Stage 3: No modification of the vision encoder is required, and GOT is customized to new character recognition features.

3.2 Pre-train the OCR-earmarked Vision Encoder

As aforementioned, GOT enjoys the encoder-decoder structure. Inspired by the LVLMs design, the decoder can be initialized by a well-trained language model. However, we did not find a suitable pre-trained encoder for an OCR-2.0 model, so we must train one ourselves. We hope the new OCR encoder can work well on commonly used scene and document text recognition in various input shapes (both slices and whole pages).

3.2.1 The Vision Encoder Generation.

The encoder structure we selected is VitDet [17] (base version with about 80M parameters) due to its local attention can greatly reduce the computational cost of high-resolution images. We follow the Vary-tiny setting [46] to design the last two layers of the encoder, which will transfer a 1024×1024×3 input image to 256×1024 image tokens. Then, these image tokens are projected into language model (OPT-125M [53]) dimension via a 1024×768 linear layer. Unlike the Vary encoder which only focuses on a single document task under a relatively unitary input shape, we incorporated natural scenes and cropped slices during our pre-training. In the pre-processing stage, images of each shape are directly resized to 1024×1024 squares, as square shapes can be used to adapt to images of various aspect ratios with a compromise.

3.2.2 Data Engine Towards Encoder Pre-training

In such an encoder pre-training stage, we use about 5M image-text pairs, including 3M scene text OCR data and 2M document OCR data. Their acquisition methods are as follows:

For the natural scene data, the English and Chinese images are sampled from Laion-2B [40] and Wukong [12] datasets, respectively. Then, the pseudo ground truth in these diverse real scenes is captured using PaddleOCR [10] tools. Overall, we obtain 2M dat with half in Chinese and half in English. For text ground truth, we perform two types of processing: 1) remove the bounding box and combine each text content in order from top to bottom and left to right. 2) crop the text region from the original image according to the bounding box and save it as image slices. The later method 2) allows us to obtain another 1M slice-type image-text pairs.

For the document-level data, we first collect open-source PDF-style files from the Common Crawl and employ the Fitz Python package to extract corresponding dense text content. In such a process, we gain 1.2M full-page PDF-style image-text pairs and 0.8M image slice data. The slice data, including line- and paragraph-level, is cropped from the PDF image via the parsed bounding box.

3.3 Scaling Up the OCR-2.0 Knowledge via Multi-task Joint-training

3.3.1 The Final Architecture of GOT

After the pre-training step of the vision encoder, we connect it to a larger language model with more powerful capabilities to build the final architecture of GOT. Here, we adopt the Qwen [4] with 500M parameters as the decoder because it has a relatively small number of parameters while incorporating prior knowledge of multiple languages. The dimension of the connector (i.e., the linear embedding layer) is adjusted into 1024×1024 to align with the input channels of the Qwen-0.5B. Hence, GOT enjoys the seamless encoder-decoder paradigm with about 580M parameters in total, which is more computationally resource-friendly and easier to deploy on a consumer-grade GPU with 4G memory. The high compression rate (1024×1024 optical pixels to 256 image tokens) of the encoder saves a lot of token space for the decoder to generate new tokens. Meanwhile, the satisfactory decoding context length (we use about 8K max-length) of the decoder ensures that the GOT can effectively output OCR results under dense scenes.

3.3.2 Data Engine for Joint-training

To inject sufficient OCR-2.0 knowledge into GOT, instead of the above-mentioned plain OCR data, we carefully explore several synthesis methods and data engines in this stage, as shown in Figure 3. We will delve into the details of each type of synthetic data in the following paragraphs.

Plain OCR data. We use 80% of the data mentioned in Section 3.2.2 as plain OCR data. To further enhance the robustness of GOT, we also add the handwritten text recognition sub-task, which involves various styles of handwriting from letters and diaries in different languages. We collect the Chinese CASIA-HWDB2 [1], English IAM [2], and Norwegian NorHand-v3 [3] datasets to meet our requirements. For the original image-text pairs with the line-level slice format, 6∼8 pairs are grouped and randomly pasted into a blank document page to achieve longer-text handwriting recognition and improve training efficiency.

Mathpix-markdown formatted data. Preserving the optical content format is critical to maintaining strong readability for the output results, especially for mathematical formulas and tables. To this end, we use multiple approaches to gather as much formatted data as possible. The details of data collection and production are as follows:

- **Math formulas.** We crawl a large number of LaTeX source *.tex* files on Arxiv and extract about 1M formula fragments from them. Next, we transfer the formula sources to Mathpix format and use the Chorme-driver to call Mathpix-markdown-it tool to render the sources to HTML format. We then convert the HTML files to SVGs and save them as PNG images. We find that this rendering method is more than 20× faster than directly using the LaTeX.
- **Molecular formulas.** We first download the *ChEMBL_25* file that contains 2M smile sources. Then we use the Mathpix-markdown-it tool and *rdkit.Chem* package to gather about 1M of molecular formula image-text pairs.
- **Table**. From the crawled *.tex* files, we extract about 0.3M table sources and render them into images. Instead of Mathpix-markdown-it, we directly utilize the LaTeX as the rendering tool due to its better rendering effects for advanced tables.
- **Full page data.** Using the Nougat [6] method, we obtain about 0.5M English markdown PDF-text pairs. Besides, following Vary [46, 47], we gather another 0.5M Chinese markdown pairs. We transfer their contents to Mathpix format. Furthermore, we additionally add 0.2M in-house data, which is directly labeled using Mathpix, including books, papers, and financial reports.

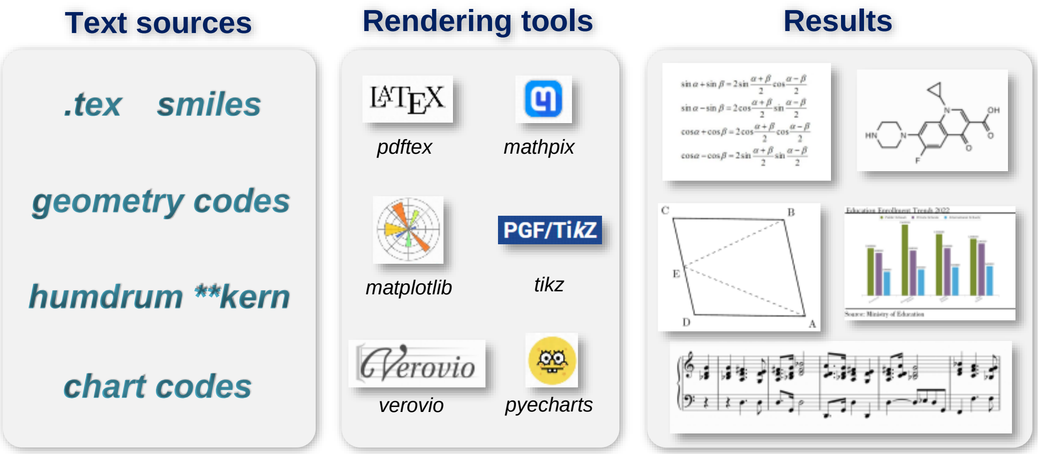

Figure 3: We use six rendering tools to run data engines to make the GOT work well on diverse OCR tasks. We utilize the LaTeX for tables, Mathpix-markdown-it for math/molecular formulas, Tikz for simple geometric shapes, Verovio for sheet music, and Matplotlib/Pyecharts for charts, respectively.

More general OCR data. We hope GOT can deal with more general optical artificial “characters”. Accordingly, we collect three related challenging tasks and generate the corresponding data. They are sheet music, geometric shapes, and charts, respectively.

- **Sheet music.** Music is a precious part of the cultural heritage and optical music recognition plays an important role in achieving automatic recognition and transcription of sheet music [7, 38]. We choose the GrandStaff [39] dataset as the source to render. The dataset of polyphonic music scores provides the *Humdrum **kern* transcriptions from the excerpts of music. In addition to the existing approximately 10w image-text samples, we also extract some text samples to re-render via the Verovio Python Package. We mainly add new backgrounds from white to real paper styles and randomly add the title and author information. Note that we only render single-system sheet music due to we don’t have professionals in the relevant field and we do not know how to assemble single-system sheets to a full page. After rendering, we collect about 0.5M samples.
- **Geometric shape.** Geometry is a key capability of LVLMs and is a necessary step towards AGI. GOT is expected to transform optical geometric elements into TikZ [34] text format. TikZ contains some concise commands to produce basic geometric elements and they can be compiled using LaTeX. We employ TikZ-style points and lines and use the simplest point-line spatial relationship to construct simple basic geometric shapes (*e.g.*, circles, rectangles, triangles, and combined shapes) as well as simple function curves (*e.g.*, straight lines, parabolas, ellipses, hyperbolas, and so on). Through this method, we obtained approximately 1M geometric Tikz data. Of course, the geometric rendering is complicated, and our current work is only a preliminary attempt. GOT can only recognize basic geometry at present, yet we believe that with the development of synthetic data technology and OCR-2.0, future models will be able to identify complex geometric shapes.
- **Chart.** Charts are crucial in data visualization and data analysis of several research fields. The proposed GOT refers to the chart structural extraction sub-task as “Chart OCR”, which converts the visual knowledge (*e.g.*, title, source, x-title, y-title, and values) on the chart image into an editable output with a table/Python-dict format. Following OneChart [8], the chart image-text pairs are rendered using Matplotlib and Pyecharts tools. Because GOT is only an OCR model, we don’t need the elements of the chart synthesized to be semantically related. Thus, we just randomly extract entity texts (for the title, source, x-title, y-title, etc) from the open-access NLP corpus. The numerical values are random numbers under a controlled distribution. Through this method, we obtained 2M chart data, with half from Matplotlib and half from Pyecharts.

3.4 Customizing New OCR Features by Post-training the Decoder

After compressing the general visual information of the diverse OCR-2.0 optical signals via the above two steps, GOT is ready to perform image-level OCR tasks in various scenarios. Based on this perceptually savvy vision encoder, GOT can be easily tuned to meet the users' needs for input and output. Here, we customize GOT to enable three new features, i.e., fine-grained, multi-page, and dynamic resolution OCR, by only post-training the decoder part.

3.4.1 Fine-grained Data Engine for Interactive OCR.

As a high-interactivity feature, fine-grained OCR [20] is the region-level visual perception controlled by spatial coordinates or colors. The user can add box coordinates (box-guided OCR) or color text (color-guided OCR) in the question prompt to request recognition within the region of interest (RoI), avoiding the output of other irrelevant characters. For the natural fine-grained OCR, the source images and annotations are from opensource datasets, including RCTW [41], ReCTS [25], and ShopSign [51], and COCO-Text [44] dataset. The datasets mentioned above provide the text bounding boxes, so we can use them to produce fine-grained (region/color prompt) OCR data directly. For the document-level fine-grained OCR, following Fox [20], we filter out those with the scanned format in the downloaded PDF files and parse the left part using Python packages (Fitz/PDFminer). We record the page-level images, bounding boxes of each line/paragraph, and the corresponding texts to produce the ground truth of the box-guided OCR sub-task. For such a task, each coordinate value is first normalized and then magnified 1000 times. For the color-guided task, we choose the most commonly used colors (red, green, and blue) as the frame colors and draw them via the corresponding bounding box on the original image. Overall, we gather about 60w samples.

3.4.2 Multi-crop Data Engine for Ultra-large-image OCR.

GOT supports 1024×1024 input resolution, which is enough for commonly used OCR tasks, e.g., scene OCR or A4-page PDF OCR. However, dynamic resolution is required for some scenes with huge images, such as two-page PDF horizontal stitching (commonly occurring when reading papers). Thanks to our high compression rate encoder, the dynamic resolution of GOT is achieved under a large sliding window (1024×1024), ensuring that our model can complete extreme resolution OCR tasks with acceptable image tokens. We use the InternVL-1.5 [9] cropping method with tiles max to 12. The ultra-resolution images are synthesized using the single-page PDF data mentioned above, including horizontal and vertical stitching. Through this method, we obtained a total of 50w image-texts pairs.

3.4.3 Multi-page Data Engine for Batched PDF-file OCR.

For OCR tasks, it is reasonable to use a "for loop" for multi-page processing. We introduce the multi-page OCR (without "for loop") feature for GOT due to some formatted PDF data making it difficult to break pages (to obtain text that is completely incompatible with each page) to further scale up, such as *.tex* in Arxiv. We hope that with GOT, researchers no longer have to worry about PDF ground truth page breaks (e.g., Nougat [6]), as they can train on multiple pages directly. To realize such a feature, we randomly sample 2-8 pages from our Mathpix formatted PDF data and join them together to form a single round OCR task. Each selected page contains text that is less than 650 tokens, to ensure that the overall length does not exceed 8K. In total, we generate about 20w multi-page OCR data, most of which are interlaced between Chinese and English pages.

4 Experiments

4.1 Implement Details

We use 8×8 L40s GPUs to train GOT. In the pre-training stage, we optimize all model parameters with a global batch size of 128 and train for 3 epochs. We utilize the AdamW [29] optimizer and a cosine annealing scheduler [28] with a start learning rate of 1e-4. The max token length in this stage is set to 4096. In the joint-training stage, we put the max token length to 6000 and train the model with the same optimizer settings as stage 1 for 1 epoch. In the last post-training stage, we expand the max token length to 8192 to allow the model to support multi-patch/page OCR features. In this stage, the beginning learning rate is 2e-5, and the epoch is set to 1.

During each train-data process, 80% of the data from the previous stage is sampled for the following stage to ensure that the basic ability does not degrade when adding new features.

Method	Size	Edit Distance↓		F1-score↑		Precision↑		Recall↑		BLEU↑		METEOR↑	
		en	zh	en	zh	en	zh	en	zh	en	zh	en	zh
UReader [50]	7B	0.718	-	0.344	-	0.296	-	0.469	-	0.103	-	0.287	-
LLaVA-NeXT [23]	34B	0.430	-	0.647	-	0.573	-	0.881	-	0.478	-	0.582	-
InternVL-ChatV1.5[9]	26B	0.393	0.265	0.751	0.816	0.698	0.784	0.917	0.866	0.568	0.622	0.663	0.717
Nougat [6]	250M	0.255	-	0.745	-	0.720	-	0.809	-	0.665	-	0.761	-
TextMonkey [27]	7B	0.265	-	0.821	-	0.778	-	0.906	-	0.671	-	0.762	-
DocOwl1.5 [13]	7B	0.258	-	0.862	-	0.835	-	0.962	-	0.788	-	0.858	-
Vary [46]	7B	0.092	0.113	0.918	0.952	0.906	0.961	0.956	0.944	0.885	0.754	0.926	0.873
Vary-toy [47]	1.8B	0.082	0.142	0.924	0.914	0.919	0.928	0.938	0.907	0.889	0.718	0.929	0.832
Qwen-VL-Plus [5]	-	0.096	0.121	0.931	0.895	0.921	0.903	0.950	0.890	0.893	0.684	0.936	0.828
Qwen-VL-Max [5]	>72B	0.057	0.091	0.964	0.931	0.955	0.917	**0.977**	0.946	0.942	0.756	**0.971**	0.885
Fox [20]	1.8B	0.046	0.061	0.952	0.954	0.957	0.964	0.948	0.946	0.930	0.842	0.954	0.908
GOT	580M	**0.035**	**0.038**	**0.972**	**0.980**	**0.971**	**0.982**	0.973	**0.978**	**0.947**	**0.878**	0.958	**0.939**

Table 1: Performance comparison of dense English (en) and Chinese (zh) OCR on document-level pages. The results of other models are from the previous work [20].

4.2 Main Results

In this section, we verify the performance of GOT on 5 different OCR tasks, including 1) plain document OCR; 2) scene text OCR; 3) fine-grained document OCR; 4) formatted (Mathpix markdown) document OCR; 5) more general character OCR. Note that the test data for each benchmark undergoes strict text similarity filtering to ensure that it is not included in the training data. Sources of each test benchmark and model performance analysis are as follows.

4.2.1 Plain document OCR performance

We use the open-source Fox [20] benchmark to test the performance of GOT on both Chinese and English PDF OCR. The metrics we used are those commonly in OCR tasks, i.e., edict distance, F1-score, precision, recall, BLEU, and METEOR. Due to the lengthy text of the document, we use word-level segmentation to calculate each indicator. As shown in Table 1, with only 580M, GOT achieves advanced performance on pure text OCR in the document, proving the excellent PDF text perception and recognition ability.

Method	Size	Edit Distance↓		F1-score↑		Precision↑		Recall↑		BLEU↑		METEOR↑	
		en	zh	en	zh	en	zh	en	zh	en	zh	en	zh
UReader [50]	7B	0.568	-	0.661	-	0.843	-	0.569	-	0.258	-	0.488	-
LLaVA-NeXT [23]	34B	0.499	-	0.558	-	0.637	-	0.538	-	0.379	-	0.678	-
TextMonkey [27]	7B	0.331	-	0.743	-	0.827	-	0.710	-	0.521	-	0.728	-
DocOwl1.5 [13]	7B	0.334	-	0.788	-	0.887	-	0.751	-	0.525	-	0.708	-
InternVL-ChatV1.5[9]	26B	0.267	0.123	0.834	0.913	**0.942**	**0.934**	0.790	0.902	0.587	0.588	0.744	0.876
Qwen-VL-Max [5]	>72B	0.182	0.168	0.881	0.867	0.891	0.878	0.888	0.873	0.586	0.572	0.848	0.845
GOT	580M	**0.112**	**0.096**	**0.926**	**0.928**	0.934	0.914	**0.927**	**0.954**	**0.676**	**0.641**	**0.896**	**0.928**

Table 2: Performance of English (en) and Chinese (zh) OCR for scene texts.

4.2.2 Scene text OCR performance

We collect 400 natural images, half in Chinese and half in English, as the scene text OCR benchmark. All the ground truth in this benchmark are manually corrected. Because the text in the scene image is relatively short, we use character-level segmentation to calculate various metrics. As shown in Table 2, we can see that GOT also works well on natural images, demonstrating the model's excellent performance on most basic OCR tasks (both document and scene texts).

4.2.3 Formatted document OCR performance

Converting the optical PDF image to a markdown-like format is an important feature of an OCR model. To verify this ability of GOT, we carefully prepare 90 pages of samples as a high-quality benchmark. The benchmark, containing both Chinese and English document pages, is first generating pseudo-labels via Mathpix, and then manually correcting for errors. In Table 3, we can see the single-scale (1024×1024) GOT can yield satisfactory results. When we use multi-crop inference, the performance of GOT is further lifted especially on formulas and tables with small texts. The

	Types	Edit Distance↓	F1-score↑	Precision↑	Recall↑	BLEU↑	METEOR↑
Markdown document	**single:**						
	All text	0.097	0.942	0.944	0.942	0.877	0.876
	Formula	0.269	0.749	0.771	0.751	0.512	0.716
	Table	0.254	0.867	0.857	0.897	0.756	0.760
	muti-crop:						
	All text	0.086	0.953	0.948	0.960	0.896	0.903
	Formula	0.159	0.865	0.858	0.882	0.628	0.828
	Table	0.220	0.878	0.861	0.919	0.779	0.811
Geneal	Sheet music	0.046	0.939	0.963	0.939	0.900	0.923
	Geometry	0.061	0.884	0.882	0.888	0.766	0.882

Table 3: Performances of formatted document (Chinese/English) and more general OCR. Single means the input is the vanilla image and multi-crop represents the dynamic resolution strategy.

results prove the effectiveness of GOT on documents with formatted outputs. Besides, the dynamic resolution scheme is a good choice when processing higher-resolution images.

4.2.4 Fine-grained OCR performance

We report the fine-grained OCR metrics of GOT. As shown in Table 4, the GOT is overall better than Fox [20] on both the bounding box-based and color-based referential OCR tasks, indicating that our model enjoys excellent interactive OCR capabilities.

Metrics	**English**					**Chinese**			
	region			color		region		color	
	DocOwl1.5 [13]	Fox [20]	GOT	Fox [20]	GOT	Fox [20]	GOT	Fox [20]	GOT
Edit Distance ↓	0.435	0.059	**0.041**	0.064	**0.034**	0.042	**0.033**	0.114	**0.040**
F1-score ↑	0.670	0.957	**0.970**	0.940	**0.966**	0.955	**0.965**	0.884	**0.957**
Precision ↑	0.886	0.962	**0.973**	0.942	**0.970**	0.966	**0.974**	0.902	**0.969**
Recall ↑	0.617	0.955	**0.969**	0.942	**0.964**	0.947	**0.958**	0.873	**0.948**
BLEU ↑	0.478	0.914	**0.926**	0.868	**0.910**	0.885	**0.898**	0.778	**0.884**
METEOR ↑	0.569	0.955	**0.966**	0.938	**0.961**	0.934	**0.942**	0.848	**0.931**

Table 4: Comparison of fine-grained document OCR.

	Metric	Deplot (1.3B) [22]	UniChart (0.26B) [31]	ChartVLM (7.3B) [48]	GPT-4V (>100B) [36]	Qwen-VL (>72B) [5]	**GOT** (0.58B)
ChartQA-SE	AP@strict	0.614	0.423	0.718	0.504	0.586	**0.747**
	AP@slight	0.709	53.18	0.814	0.606	0.685	**0.845**
	AP@high	0.729	0.560	0.842	0.643	0.727	**0.867**
PlotQA-SE	AP@strict	0.031	0.105	0.038	0.073	0.005	**0.133**
	AP@slight	16.49	0.260	0.468	0.194	0.042	**0.596**
	AP@high	26.50	0.269	0.540	0.223	0.120	**0.640**

Table 5: Performance comparisons on number-centric chart OCR.

4.2.5 More general OCR performance

We utilize the sheet music, geometry, and chart benchmarks to verify GOT's more general OCR performance. For the first two tasks, we separately render 100 and 180 additional samples as benchmarks, and as can be seen in Table 3, GOT still performs well on these new OCR tasks. For chart OCR, we use structure-extraction version [8] ChartQA [32] and PlotQA [35] as benchmarks. In Table 5, the chart OCR ability of GOT is even much better than the chart-specific models and popular LVLMs. All results demonstrate the effectiveness of our model on more general OCR tasks.

5 Conclusion

This paper presents a primary OCR-2.0 model that is structurally simpler than OCR-1.0 systems, focuses more on pure OCR tasks than LVLMs, and enjoys superior performance. OCR-2.0 integrates various pan-OCR tasks into one model and is a valuable research direction in model design, data engineering, and application scenarios. We want the simple, elegant, effective, and promising GOT OCR-2.0 model to attract more attention to such a task.

6 Appendix

In this section, we provide sufficient output results of GOT to show its outstanding OCR performance. We also demonstrate the format of the corresponding input prompt for different types of OCR tasks.

Prompt: OCR with format:

Output:

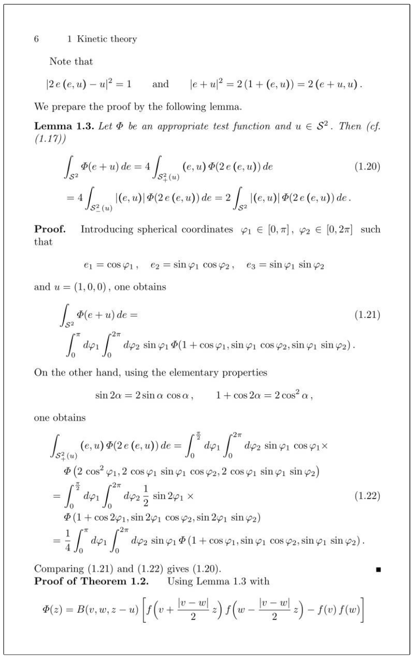

6 1 Kinetic theory

Note that

$$|2\,e\,(e,u)-u|^2=1 \qquad \text{and} \qquad |e+u|^2=2\,(1+(e,u))=2\,(e+u,u)\,.$$

We prepare the proof by the following lemma.

Lemma 1.3. *Let $\varPhi$ be an appropriate test function and $u \in \mathcal{S}^2$. Then (cf. (1.17))*

$$\begin{aligned}\int_{\mathcal{S}^2}\varPhi(e+u)\,de &= 4\int_{\mathcal{S}^2_+(u)}(e,u)\,\varPhi(2\,e\,(e,u))\,de \qquad (1.20)\\ &= 4\int_{\mathcal{S}^2_-(u)}|(e,u)|\,\varPhi(2\,e\,(e,u))\,de = 2\int_{\mathcal{S}^2}|(e,u)|\,\varPhi(2\,e\,(e,u))\,de\,.\end{aligned}$$

Proof. Introducing spherical coordinates $\varphi_1 \in [0,\pi]\,,\ \varphi_2 \in [0,2\pi]$ such that

$$e_1=\cos\varphi_1\,,\quad e_2=\sin\varphi_1\,\cos\varphi_2\,,\quad e_3=\sin\varphi_1\,\sin\varphi_2$$

and $u=(1,0,0)$, one obtains

$$\begin{aligned}&\int_{\mathcal{S}^2}\varPhi(e+u)\,de = \qquad (1.21)\\ &\int_0^{\pi}d\varphi_1\int_0^{2\pi}d\varphi_2\,\sin\varphi_1\,\varPhi(1+\cos\varphi_1,\sin\varphi_1\,\cos\varphi_2,\sin\varphi_1\,\sin\varphi_2)\,.\end{aligned}$$

On the other hand, using the elementary properties

$$\sin 2\alpha = 2\sin\alpha\,\cos\alpha\,, \qquad 1+\cos 2\alpha = 2\cos^2\alpha\,,$$

one obtains

$$\begin{aligned}\int_{\mathcal{S}^2_+(u)}&(e,u)\,\varPhi(2\,e\,(e,u))\,de = \int_0^{\frac{\pi}{2}}d\varphi_1\int_0^{2\pi}d\varphi_2\,\sin\varphi_1\,\cos\varphi_1\times\\ &\varPhi\left(2\,\cos^2\varphi_1,2\,\cos\varphi_1\,\sin\varphi_1\,\cos\varphi_2,2\,\cos\varphi_1\,\sin\varphi_1\,\sin\varphi_2\right)\\ =&\int_0^{\frac{\pi}{2}}d\varphi_1\int_0^{2\pi}d\varphi_2\,\frac{1}{2}\,\sin 2\varphi_1\times \qquad (1.22)\\ &\varPhi\left(1+\cos 2\varphi_1,\sin 2\varphi_1\,\cos\varphi_2,\sin 2\varphi_1\,\sin\varphi_2\right)\\ =&\frac{1}{4}\int_0^{\pi}d\varphi_1\int_0^{2\pi}d\varphi_2\,\sin\varphi_1\,\varPhi\left(1+\cos\varphi_1,\sin\varphi_1\,\cos\varphi_2,\sin\varphi_1\,\sin\varphi_2\right)\,.\end{aligned}$$

Comparing (1.21) and (1.22) gives (1.20). ■

Proof of Theorem 1.2. Using Lemma 1.3 with

$$\varPhi(z)=B(v,w,z-u)\left[f\Big(v+\frac{|v-w|}{2}\,z\Big)\,f\Big(w-\frac{|v-w|}{2}\,z\Big)-f(v)\,f(w)\right]$$

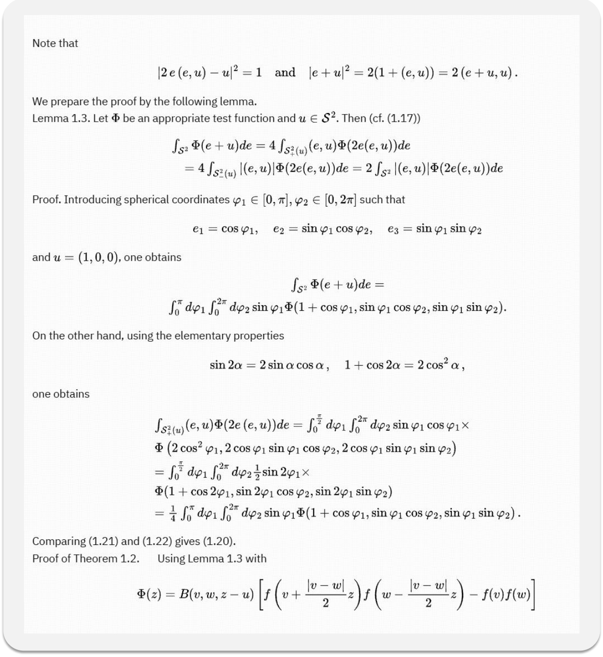

Note that

$$|2\,e\,(e,u)-u|^2=1 \quad \text{and} \quad |e+u|^2=2(1+(e,u))=2\,(e+u,u)\,.$$

We prepare the proof by the following lemma.
Lemma 1.3. Let Φ be an appropriate test function and $u \in \mathcal{S}^2$. Then (cf. (1.17))

$$\begin{aligned}\textstyle\int_{\mathcal{S}^2}\Phi(e+u)de &= \textstyle 4\int_{\mathcal{S}^2_+(u)}(e,u)\Phi(2e(e,u))de\\ &= \textstyle 4\int_{\mathcal{S}^2_-(u)}|(e,u)|\Phi(2e(e,u))de = 2\int_{\mathcal{S}^2}|(e,u)|\Phi(2e(e,u))de\end{aligned}$$

Proof. Introducing spherical coordinates $\varphi_1 \in [0,\pi], \varphi_2 \in [0,2\pi]$ such that

$$e_1=\cos\varphi_1, \quad e_2=\sin\varphi_1\cos\varphi_2, \quad e_3=\sin\varphi_1\sin\varphi_2$$

and $u=(1,0,0)$, one obtains

$$\begin{gathered}\textstyle\int_{\mathcal{S}^2}\Phi(e+u)de=\\ \textstyle\int_0^{\pi}d\varphi_1\int_0^{2\pi}d\varphi_2\sin\varphi_1\Phi(1+\cos\varphi_1,\sin\varphi_1\cos\varphi_2,\sin\varphi_1\sin\varphi_2).\end{gathered}$$

On the other hand, using the elementary properties

$$\sin 2\alpha = 2\sin\alpha\cos\alpha\,, \quad 1+\cos 2\alpha = 2\cos^2\alpha\,,$$

one obtains

$$\begin{aligned}&\textstyle\int_{\mathcal{S}^2_+(u)}(e,u)\Phi(2e\,(e,u))de=\int_0^{\frac{\pi}{2}}d\varphi_1\int_0^{2\pi}d\varphi_2\sin\varphi_1\cos\varphi_1\times\\ &\Phi\left(2\cos^2\varphi_1,2\cos\varphi_1\sin\varphi_1\cos\varphi_2,2\cos\varphi_1\sin\varphi_1\sin\varphi_2\right)\\ &\textstyle=\int_0^{\frac{\pi}{2}}d\varphi_1\int_0^{2\pi}d\varphi_2\frac{1}{2}\sin 2\varphi_1\times\\ &\Phi(1+\cos 2\varphi_1,\sin 2\varphi_1\cos\varphi_2,\sin 2\varphi_1\sin\varphi_2)\\ &\textstyle=\frac{1}{4}\int_0^{\pi}d\varphi_1\int_0^{2\pi}d\varphi_2\sin\varphi_1\Phi(1+\cos\varphi_1,\sin\varphi_1\cos\varphi_2,\sin\varphi_1\sin\varphi_2)\,.\end{aligned}$$

Comparing (1.21) and (1.22) gives (1.20).
Proof of Theorem 1.2. Using Lemma 1.3 with

$$\Phi(z)=B(v,w,z-u)\left[f\left(v+\frac{|v-w|}{2}z\right)f\left(w-\frac{|v-w|}{2}z\right)-f(v)f(w)\right]$$

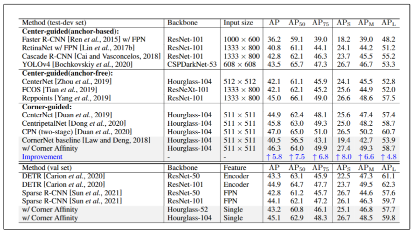

Method (test-dev set)	Backbone	Input size	AP	AP_{50}	AP_{75}	AP_S	AP_M	AP_L
Center-guided(anchor-based):								
Faster R-CNN [Ren *et al.*, 2015] w/ FPN	ResNet-101	1000 × 600	36.2	59.1	39.0	18.2	39.0	48.2
RetinaNet w/ FPN [Lin *et al.*, 2017b]	ResNet-101	1333 × 800	40.8	61.1	44.1	24.1	44.2	51.2
Cascade R-CNN [Cai and Vasconcelos, 2018]	ResNet-101	1333 × 800	42.8	62.1	46.3	23.7	45.5	55.2
YOLOv4 [Bochkovskiy *et al.*, 2020]	CSPDarkNet-53	608 × 608	43.5	65.7	47.3	26.7	46.7	53.3
Center-guided(anchor-free):								
CenterNet [Zhou *et al.*, 2019]	Hourglass-104	512 × 512	42.1	61.1	45.9	24.1	45.5	52.8
FCOS [Tian *et al.*, 2019]	ResNeXt-101	1333 × 800	42.1	62.1	45.2	25.6	44.9	52.0
Reppoints [Yang *et al.*, 2019]	ResNet-101	1333 × 800	45.0	66.1	49.0	26.6	48.6	57.5
Corner-guided:								
CenterNet [Duan *et al.*, 2019]	Hourglass-104	511 × 511	44.9	62.4	48.1	25.6	47.4	57.4
CentripetalNet [Dong *et al.*, 2020]	Hourglass-104	511 × 511	45.8	63.0	49.3	25.0	48.2	58.7
CPN (two-stage) [Duan *et al.*, 2020]	Hourglass-104	511 × 511	47.0	65.0	51.0	26.5	50.2	60.7
CornerNet baseline [Law and Deng, 2018]	Hourglass-104	511 × 511	40.5	56.5	43.1	19.4	42.7	53.9
w/ Corner Affinity	Hourglass-104	511 × 511	46.3	64.0	49.9	27.4	49.3	58.7
Improvement	-	-	↑ 5.8	↑ 7.5	↑ 6.8	↑ 8.0	↑ 6.6	↑ 4.8
Method (val set)	Backbone	Feature	AP	AP_{50}	AP_{75}	AP_S	AP_M	AP_L
DETR [Carion *et al.*, 2020]	ResNet-50	Encoder	43.3	63.1	45.9	22.5	47.3	61.1
DETR [Carion *et al.*, 2020]	ResNet-101	Encoder	44.9	64.7	47.7	23.7	49.5	62.3
Sparse R-CNN [Sun *et al.*, 2021]	ResNet-50	FPN	42.8	61.2	45.7	26.7	44.6	57.6
Sparse R-CNN [Sun *et al.*, 2021]	ResNet-101	FPN	44.1	62.1	47.2	26.1	46.3	59.7
w/ Corner Affinity	Hourglass-52	Single	43.2	60.8	46.1	25.1	46.8	57.7
w/ Corner Affinity	Hourglass-104	Single	45.1	62.9	48.3	26.7	48.5	59.8

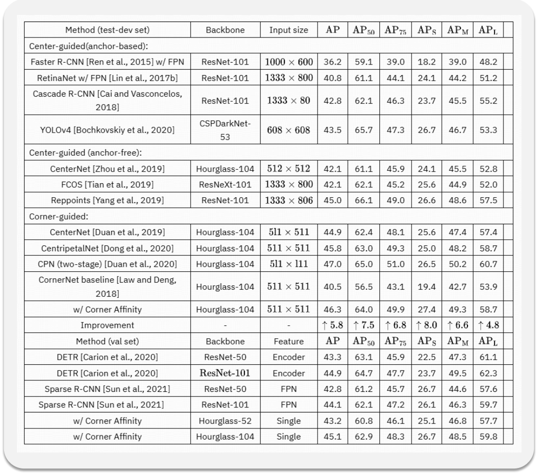

Method (test-dev set)	Backbone	Input size	AP	AP_{50}	AP_{75}	AP_S	AP_M	AP_L	
Center-guided(anchor-based):									
Faster R-CNN [Ren et al., 2015] w/ FPN	ResNet-101	1000×600	36.2	59.1	39.0	18.2	39.0	48.2	
RetinaNet w/ FPN [Lin et al., 2017b]	ResNet-101	1333×800	40.8	61.1	44.1	24.1	44.2	51.2	
Cascade R-CNN [Cai and Vasconcelos, 2018]	ResNet-101	1333×80	42.8	62.1	46.3	23.7	45.5	55.2	
YOLOv4 [Bochkovskiy et al., 2020]	CSPDarkNet-53	608×608	43.5	65.7	47.3	26.7	46.7	53.3	
Center-guided (anchor-free):									
CenterNet [Zhou et al., 2019]	Hourglass-104	512×512	42.1	61.1	45.9	24.1	45.5	52.8	
FCOS [Tian et al., 2019]	ResNeXt-101	1333×800	42.1	62.1	45.2	25.6	44.9	52.0	
Reppoints [Yang et al., 2019]	ResNet-101	1333×806	45.0	66.1	49.0	26.6	48.6	57.5	
Corner-guided:									
CenterNet [Duan et al., 2019]	Hourglass-104	$5l1 \times 511$	44.9	62.4	48.1	25.6	47.4	57.4	
CentripetalNet [Dong et al., 2020]	Hourglass-104	511×511	45.8	63.0	49.3	25.0	48.2	58.7	
CPN (two-stage) [Duan et al., 2020]	Hourglass-104	$5l1 \times l11$	47.0	65.0	51.0	26.5	50.2	60.7	
CornerNet baseline [Law and Deng, 2018]	Hourglass-104	511×511	40.5	56.5	43.1	19.4	42.7	53.9	
w/ Corner Affinity	Hourglass-104	511×511	46.3	64.0	49.9	27.4	49.3	58.7	
Improvement	-	-	$\uparrow 5.8$	$\uparrow 7.5$	$\uparrow 6.8$	$\uparrow 8.0$	$\uparrow 6.6$	$\uparrow 4.8$	
Method (val set)	Backbone	Feature	AP	AP_{50}	AP_{75}	AP_S	AP_M	AP_L	
DETR [Carion et al., 2020]	ResNet-50	Encoder	43.3	63.1	45.9	22.5	47.3	61.1	
DETR [Carion et al., 2020]	ResNet-101	Encoder	44.9	64.7	47.7	23.7	49.5	62.3	
Sparse R-CNN [Sun et al., 2021]	ResNet-50	FPN	42.8	61.2	45.7	26.7	44.6	57.6	
Sparse R-CNN [Sun et al., 2021]	ResNet-101	FPN	44.1	62.1	47.2	26.1	46.3	59.7	
w/ Corner Affinity	Hourglass-52	Single	43.2	60.8	46.1	25.1	46.8	57.7	
w/ Corner Affinity	Hourglass-104	Single	45.1	62.9	48.3	26.7	48.5	59.8	

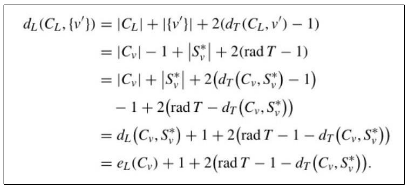

$$\begin{aligned}d_L(C_L,\{v'\}) &= |C_L|+|\{v'\}|+2(d_T(C_L,v')-1)\\ &= |C_v|-1+|S_v^*|+2(\operatorname{rad}T-1)\\ &= |C_v|+|S_v^*|+2(d_T(C_v,S_v^*)-1)\\ &\quad -1+2(\operatorname{rad}T-d_T(C_v,S_v^*))\\ &= d_L(C_v,S_v^*)+1+2(\operatorname{rad}T-1-d_T(C_v,S_v^*))\\ &= e_L(C_v)+1+2(\operatorname{rad}T-1-d_T(C_v,S_v^*)).\end{aligned}$$

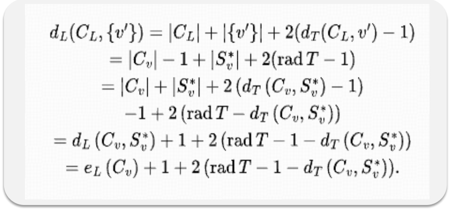

$$\begin{gathered}d_L(C_L,\{v'\}) = |C_L|+|\{v'\}|+2(d_T(C_L,v')-1)\\ =|C_v|-1+|S_v^*|+2(\operatorname{rad}T-1)\\ =|C_v|+|S_v^*|+2\left(d_T\left(C_v,S_v^*\right)-1\right)\\ -1+2\left(\operatorname{rad}T-d_T\left(C_v,S_v^*\right)\right)\\ =d_L\left(C_v,S_v^*\right)+1+2\left(\operatorname{rad}T-1-d_T\left(C_v,S_v^*\right)\right)\\ =e_L\left(C_v\right)+1+2\left(\operatorname{rad}T-1-d_T\left(C_v,S_v^*\right)\right).\end{gathered}$$

Figure 4: The formatted text OCR ability of GOT. GOT works well on full-page texts and table/formula slice texts. These input forms are the most commonly used in document OCR, which proves that GOT has great prospects in application.

Prompt: OCR:

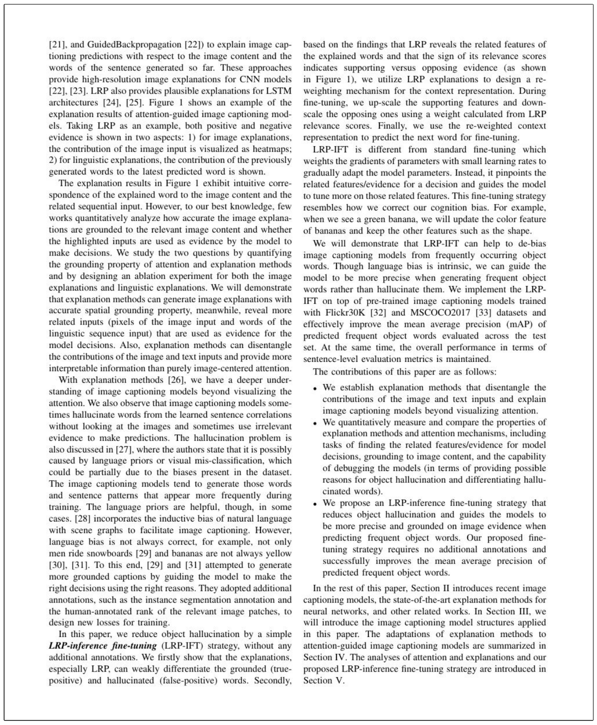

[21], and GuidedBackpropagation [22]) to explain image captioning predictions with respect to the image content and the words of the sentence generated so far. These approaches provide high-resolution image explanations for CNN models [22], [23]. LRP also provides plausible explanations for LSTM architectures [24], [25]. Figure 1 shows an example of the explanation results of attention-guided image captioning models. Taking LRP as an example, both positive and negative evidence is shown in two aspects: 1) for image explanations, the contribution of the image input is visualized as heatmaps; 2) for linguistic explanations, the contribution of the previously generated words to the latest predicted word is shown.

The explanation results in Figure 1 exhibit intuitive correspondence of the explained word to the image content and the related sequential input. However, to our best knowledge, few works quantitatively analyze how accurate the image explanations are grounded to the relevant image content and whether the highlighted inputs are used as evidence by the model to make decisions. We study the two questions by quantifying the grounding property of attention and explanation methods and by designing an ablation experiment for both the image explanations and linguistic explanations. We will demonstrate that explanation methods can generate image explanations with accurate spatial grounding property, meanwhile, reveal more related inputs (pixels of the image input and words of the linguistic sequence input) that are used as evidence for the model decisions. Also, explanation methods can disentangle the contributions of the image and text inputs and provide more interpretable information than purely image-centered attention.

With explanation methods [26], we have a deeper understanding of image captioning models beyond visualizing the attention. We also observe that image captioning models sometimes hallucinate words from the learned sentence correlations without looking at the images and sometimes use irrelevant evidence to make predictions. The hallucination problem is also discussed in [27], where the authors state that it is possibly caused by language priors or visual mis-classification, which could be partially due to the biases present in the dataset. The image captioning models tend to generate those words and sentence patterns that appear more frequently during training. The language priors are helpful, though, in some cases. [28] incorporates the inductive bias of natural language with scene graphs to facilitate image captioning. However, language bias is not always correct, for example, not only men ride snowboards [29] and bananas are not always yellow [30], [31]. To this end, [29] and [31] attempted to generate more grounded captions by guiding the model to make the right decisions using the right reasons. They adopted additional annotations, such as the instance segmentation annotation and the human-annotated rank of the relevant image patches, to design new losses for training.

In this paper, we reduce object hallucination by a simple ***LRP-inference fine-tuning*** (LRP-IFT) strategy, without any additional annotations. We firstly show that the explanations, especially LRP, can weakly differentiate the grounded (true-positive) and hallucinated (false-positive) words. Secondly, based on the findings that LRP reveals the related features of the explained words and that the sign of its relevance scores indicates supporting versus opposing evidence (as shown in Figure 1), we utilize LRP explanations to design a re-weighting mechanism for the context representation. During fine-tuning, we up-scale the supporting features and down-scale the opposing ones using a weight calculated from LRP relevance scores. Finally, we use the re-weighted context representation to predict the next word for fine-tuning.

LRP-IFT is different from standard fine-tuning which weights the gradients of parameters with small learning rates to gradually adapt the model parameters. Instead, it pinpoints the related features/evidence for a decision and guides the model to tune more on those related features. This fine-tuning strategy resembles how we correct our cognition bias. For example, when we see a green banana, we will update the color feature of bananas and keep the other features such as the shape.

We will demonstrate that LRP-IFT can help to de-bias image captioning models from frequently occurring object words. Though language bias is intrinsic, we can guide the model to be more precise when generating frequent object words rather than hallucinate them. We implement the LRP-IFT on top of pre-trained image captioning models trained with Flickr30K [32] and MSCOCO2017 [33] datasets and effectively improve the mean average precision (mAP) of predicted frequent object words evaluated across the test set. At the same time, the overall performance in terms of sentence-level evaluation metrics is maintained.

The contributions of this paper are as follows:

- We establish explanation methods that disentangle the contributions of the image and text inputs and explain image captioning models beyond visualizing attention.
- We quantitatively measure and compare the properties of explanation methods and attention mechanisms, including tasks of finding the related features/evidence for model decisions, grounding to image content, and the capability of debugging the models (in terms of providing possible reasons for object hallucination and differentiating hallucinated words).
- We propose an LRP-inference fine-tuning strategy that reduces object hallucination and guides the models to be more precise and grounded on image evidence when predicting frequent object words. Our proposed fine-tuning strategy requires no additional annotations and successfully improves the mean average precision of predicted frequent object words.

In the rest of this paper, Section II introduces recent image captioning models, the state-of-the-art explanation methods for neural networks, and other related works. In Section III, we will introduce the image captioning model structures applied in this paper. The adaptations of explanation methods to attention-guided image captioning models are summarized in Section IV. The analyses of attention and explanations and our proposed LRP-inference fine-tuning strategy are introduced in Section V.

Output:

[21], and GuidedBackpropagation [22]) to explain image captioning predictions with respect to the image content and the words of the sentence generated so far. These approaches provide high-resolution image explanations for CNN models [22], [23], LRP also provides plausible explanations for LSTM architectures [24], [25]. Figure 1 shows an example of the explanation results of attention-guided image captioning models. Taking LRP as an example, both positive and negative evidence is shown in two aspects: 1) for image explanations, the contribution of the image input is visualized as heatmaps; 2) for linguistic explanations, the contribution of the previously generated words to the latest predicted word is shown.

The explanation results in Figure 1 exhibit intuitive corresspondence of the explained word to the image content and the related sequential input. However, to our best knowledge, few works quantitatively analyze how accurate the image explanations are grounded to the relevant image content and whether the highlighted inputs are used as evidence by the model to make decisions. We study the two questions by quantifying the grounding property of attention and explanation methods and by designing an ablation experiment for both the image explanations and linguistic explanations. We will demonstrate that explanation methods can generate image explanations with accurate spatial grounding property, meanwhile, reveal more related inputs (pixels of the image input and words of the linguistic sequence input) that are used as evidence for the model decisions. Also, explanation methods can disentangle the contributions of the image and text inputs and provide more interpretable information than purely image-centered attention.

With explanation methods [26], we have a deeper understanding of image captioning models beyond visualizing the attention. We also observe that image captioning models sometimes hallucinate words from the learned sentence correlations without looking at the images and sometimes use irrelevant evidence to make predictions. The hallucination problem is also discussed in [27], where the authors state that it is possibly caused by language priors or visual mis-classification, which could be partially due to the biases present in the dataset.

The image captioning models tend to generate those words and sentence patterns that appear more frequently during training. The language priors are helpful, though, in some cases. [28] incorporates the inductive bias of natural language with scene graphs to facilitate image captioning. However, language bias is not always correct, for example, not only men ride snowboards [29] and bananas are not always yellow [30], [31]. To this end, [29] and [31] attempted to generate more grounded captions by guiding the model to make the right decisions using the right reasons. They adopted additional annotations, such as the instance segmentation annotation and the human-annotated rank of the relevant image patches, to design new losses for training.

In this paper, we reduce object hallucination by a simple LRP-inference fine-tuning (LRP-IFT) strategy, without any additional annotations .We firstly show that the explanations, especially LRP, can weakly differentiate the grounded (true-positive) and hallucinated (false-positive) words. Secondly,

based on the findings that LRP reveals the related features of the explained words and that the sign of its relevance scores indicates supporting versus opposing evidence (as shown in Figure 1), we utilize LRP explanations to design a re-weighting mechanism for the context representation. During fine-tuning, we up-scale the supporting features and down-scale the opposing ones using a weight calculated from LRP relevance scores. Finally, we use the re-weighted context representation to predict the next word for fine-tuning.

LRP-IFT is different from standard fine-tuning which weights the gradients of parameters with small learning rates to gradually adapt the model parameters. Instead, it pinpoints the related features/evidence for a decision and guides the model to tune more on those related features .This fine-tuning strategy resembles how we correct our cognition bias. For example, when we see a green banana, we will update the color feature of bananas and keep the other features such as the shape.

We will demonstrate that LRP-IFT can help to de-bias image captioning models from frequently occurring object words. Though language bias is intrinsic, we can guide the model to be more precise when generating frequent object words rather than hallucinate them. We implement the LRP-IFT on top of pre-trained image captioning models trained with Flickr30K [32] and MSCOCO2017 [33] datasets and effectively improve the mean average precision (mAP) of predicted frequent object words evaluated across the test set. At the same time, the overall performance in terms of sentence-level evaluation metrics is maintained.

The contributions of this paper are as follows:

- We establish explanation methods that disentangle the contributions of the image and text inputs and explain image captioning models beyond visualizing attention.
- We quantitatively measure and compare the properties of explanation methods and attention mechanisms, including tasks of finding the related features/evidence for model decisions, grounding to image content, and the capability of debugging the models (in terms of providing possible reasons for object hallucination and differentiating hallucinated words).
- We propose an LRP-inference fine-tuning strategy that reduces object hallucination and guides the models to be more precise and grounded on image evidence when predicting frequent object words .Our proposed fine-tuning strategy requires no additional annotations and successfully improves the mean average precision of predicted frequent object words.

In the rest of this paper, Section II introduces recent image captioning models, the state-of-the-art explanation methods for neural networks, and other related works. In Section III, we will introduce the image captioning model structures applied in this paper. The adaptations of explanation methods to attention-guided image captioning models are summarized in Section IV. The analyses of attention and explanations and our proposed LRP-inference fine-tuning strategy are introduced in Section V.

Figure 5: The plain text (document) OCR ability of GOT. For double-column documents with high text density, GOT can still handle them well, proving the excellent text perception ability.

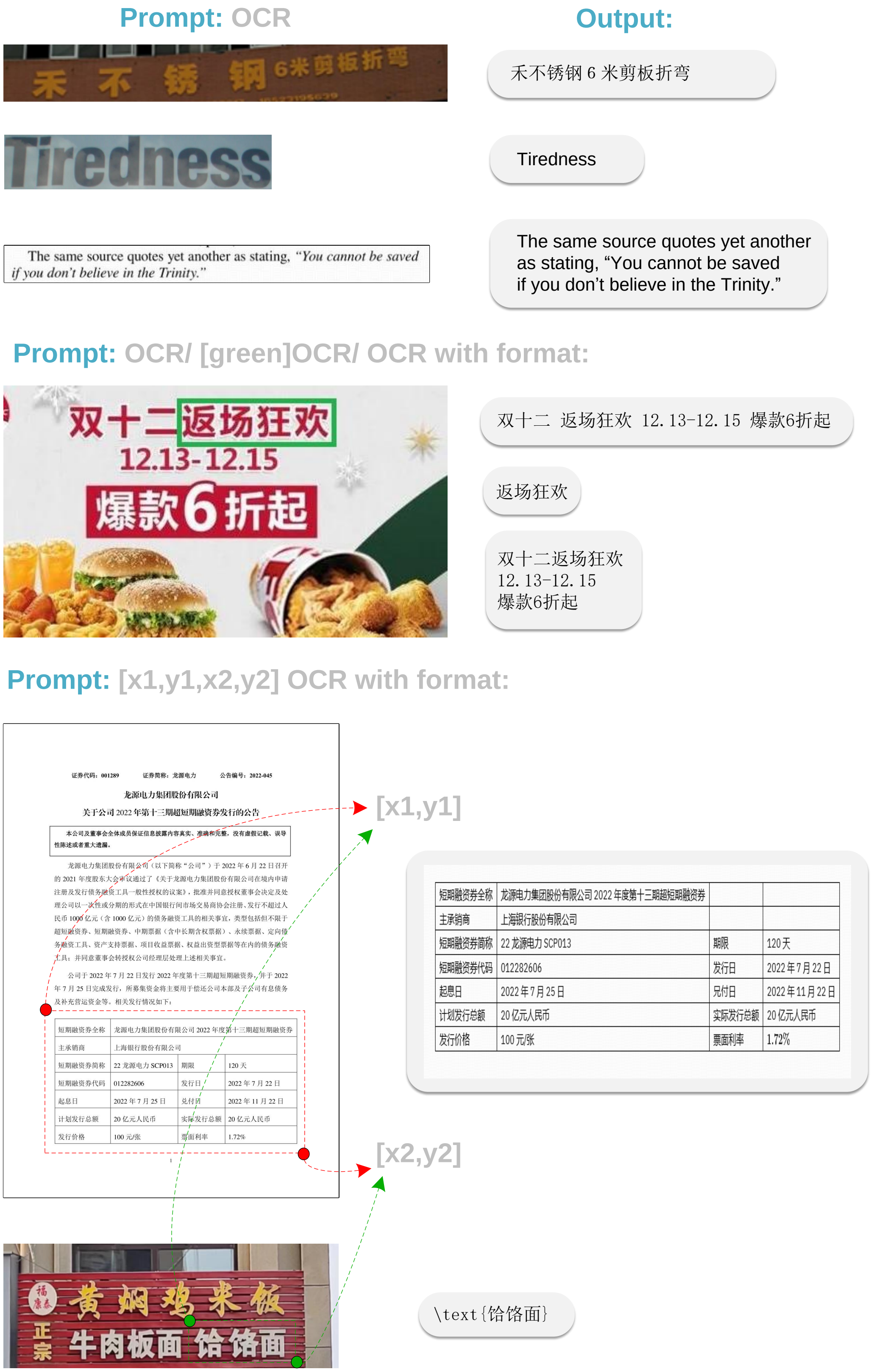

禾不锈钢 6 米剪板折弯

Tiredness

The same source quotes yet another as stating, *"You cannot be saved if you don't believe in the Trinity."*

The same source quotes yet another as stating, "You cannot be saved
if you don't believe in the Trinity."

双十二 返场狂欢 12. 13-12. 15 爆款6折起

返场狂欢

双十二返场狂欢
12. 13-12. 15
爆款6折起

证券代码：001289　　证券简称：龙源电力　　公告编号：2022-045

龙源电力集团股份有限公司

关于公司 2022 年第十三期超短期融资券发行的公告

本公司及董事会全体成员保证信息披露内容真实、准确和完整，没有虚假记载、误导性陈述或者重大遗漏。

龙源电力集团股份有限公司（以下简称"公司"）于 2022 年 6 月 22 日召开的 2021 年度股东大会审议通过了《关于龙源电力集团股份有限公司在境内申请注册及发行债务融资工具一般性授权的议案》，批准并同意授权董事会决定及处理公司以一次性或分期的形式在中国银行间市场交易商协会注册、发行不超过人民币 1000 亿元（含 1000 亿元）的债务融资工具的相关事宜，类型包括但不限于超短融资券、短期融资券、中期票据（含中长期含权票据）、永续票据、定向债务融资工具、资产支持票据、项目收益票据、权益出资型票据等在内的债务融资工具；并同意董事会转授权公司经理层处理上述相关事宜。

公司于 2022 年 7 月 22 日发行 2022 年度第十三期超短期融资券，并于 2022 年 7 月 25 日完成发行，所募集资金将主要用于偿还公司本部及子公司有息债务及补充营运资金等。相关发行情况如下：

短期融资券全称	龙源电力集团股份有限公司 2022 年度第十三期超短期融资券		
主承销商	上海银行股份有限公司		
短期融资券简称	22 龙源电力 SCP013	期限	120 天
短期融资券代码	012282606	发行日	2022 年 7 月 22 日
起息日	2022 年 7 月 25 日	兑付日	2022 年 11 月 22 日
计划发行总额	20 亿元人民币	实际发行总额	20 亿元人民币
发行价格	100 元/张	票面利率	1.72%

短期融资券全称	龙源电力集团股份有限公司2022年度第十三期超短期融资券		
主承销商	上海银行股份有限公司		
短期融资券简称	22龙源电力SCP013	期限	120天
短期融资券代码	012282606	发行日	2022年7月22日
起息日	2022年7月25日	兑付日	2022年11月22日
计划发行总额	20亿元人民币	实际发行总额	20亿元人民币
发行价格	100元/张	票面利率	1.72%

\text{饸饹面}

Figure 6: Scene OCR and fine-grained OCR results of GOT. We equip GOT with more interactive fine-grained OCR tasks, allowing it to output OCR results of regions of interest based on prompts.

Prompt: OCR with format upon the patch reference:

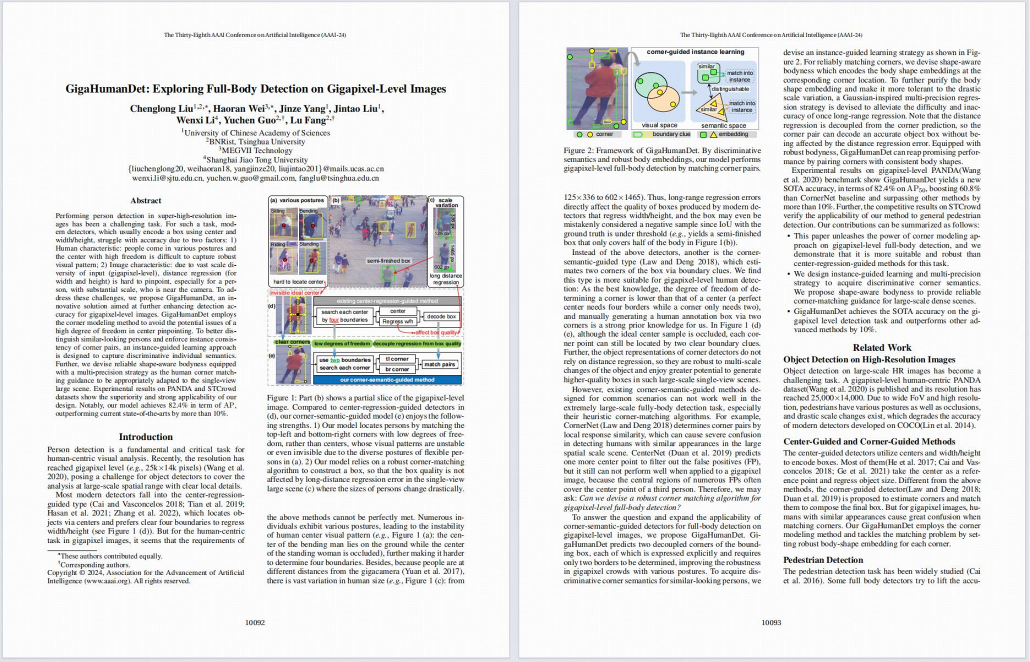

Output:

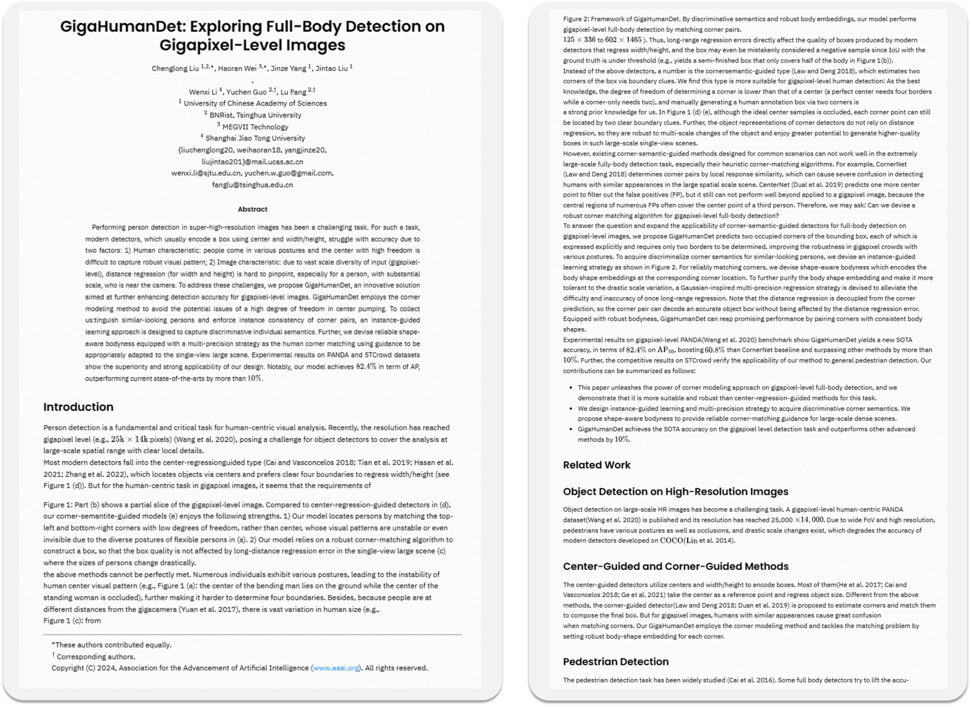

GigaHumanDet: Exploring Full-Body Detection on Gigapixel-Level Images

Chenglong Liu [1,2,*], Haoran Wei [3,*], Jinze Yang [1], Jintao Liu [1]
,
Wenxi Li [4], Yuchen Guo [2,†], Lu Fang [2,†]
[1] University of Chinese Academy of Sciences
[2] BNRist, Tsinghua University
[3] MEGVII Technology
[4] Shanghai Jiao Tong University
{liuchenglong20, weihaoran18, yangjinze20,
liujintao201}@mail.ucas.ac.cn
wenxi.li@sjtu.edu.cn, yuchen.w.guo@gmail.com,
fanglu@tsinghua.edu.cn

Abstract

Performing person detection in super-high-resolution images has been a challenging task. For such a task, modern detectors, which usually encode a box using center and width/height, struggle with accuracy due to two factors: 1) Human characteristic: people come in various postures and the center with high freedom is difficult to capture robust visual pattern; 2) Image characteristic: due to vast scale diversity of input (gigapixel-level), distance regression (for width and height) is hard to pinpoint, especially for a person, with substantial scale, who is near the camera. To address these challenges, we propose GigaHumanDet, an innovative solution aimed at further enhancing detection accuracy for gigapixel-level images. GigaHumanDet employs the corner modeling method to avoid the potential issues of a high degree of freedom in center pumping. To collect us:tinguish similar-looking persons and enforce instance consistency of corner pairs, an instance-guided learning approach is designed to capture discriminative individual semantics. Further, we devise reliable shape-aware bodyness equipped with a multi-precision strategy as the human corner matching using guidance to be appropriately adapted to the single-view large scene. Experimental results on PANDA and STCrowd datasets show the superiority and strong applicability of our design. Notably, our model achieves 82.4% in term of AP, outperforming current state-of-the-arts by more than 10%.

Introduction

Person detection is a fundamental and critical task for human-centric visual analysis. Recently, the resolution has reached gigapixel level (e.g., $25\mathrm{k} \times 14\mathrm{k}$ pixels) (Wang et al. 2020), posing a challenge for object detectors to cover the analysis at large-scale spatial range with clear local details.

Most modern detectors fall into the center-regressionguided type (Cai and Vasconcelos 2018; Tian et al. 2019; Hasan et al. 2021; Zhang et al. 2022), which locates objects via centers and prefers clear four boundaries to regress width/height (see Figure 1 (d)). But for the human-centric task in gigapixel images, it seems that the requirements of

Figure 1: Part (b) shows a partial slice of the gigapixel-level image. Compared to center-regression-guided detectors in (d), our corner-semantite-guided models (e) enjoys the following strengths. 1) Our model locates persons by matching the top-left and bottom-right corners with low degrees of freedom, rather than center, whose visual patterns are unstable or even invisible due to the diverse postures of flexible persons in (a). 2) Our model relies on a robust corner-matching algorithm to construct a box, so that the box quality is not affected by long-distance regression error in the single-view large scene (c) where the sizes of persons change drastically.

the above methods cannot be perfectly met. Numerous individuals exhibit various postures, leading to the instability of human center visual pattern (e.g., Figure 1 (a): the center of the bending man lies on the ground while the center of the standing woman is occluded), further making it harder to determine four boundaries. Besides, because people are at different distances from the gigacamera (Yuan et al. 2017), there is vast variation in human size (e.g.,
Figure 1 (c): from

*These authors contributed equally.
† Corresponding authors.
Copyright (C) 2024, Association for the Advancement of Artificial Intelligence (www.aaai.org). All rights reserved.

Figure 2: Framework of GigaHumanDet. By discriminative semantics and robust body embeddings, our model performs gigapixel-level full-body detection by matching corner pairs.

125×336 to 602×1465). Thus, long-range regression errors directly affect the quality of boxes produced by modern detectors that regress width/height, and the box may even be mistakenly considered a negative sample since IoU with the ground truth is under threshold (e.g., yields a semi-finished box that only covers half of the body in Figure 1(b)).

Instead of the above detectors, a number is the cornersemantic-guided type (Law and Deng 2018), which estimates two corners of the box via boundary clues. We find this type is more suitable for gigapixel-level human detection: As the best knowledge, the degree of freedom of determining a corner is lower than that of a center (a perfect center needs four borders while a corner-only needs two), and manually generating a human annotation box via two corners is
a strong prior knowledge for us. In Figure 1 (d) (e), although the ideal center samples is occluded, each corner point can still be located by two clear boundary clues. Further, the object representations of corner detectors do not rely on distance regression, so they are robust to multi-scale changes of the object and enjoy greater potential to generate higher-quality boxes in such large-scale single-view scenes.

However, existing corner-semantic-guided methods designed for common scenarios can not work well in the extremely large-scale fully-body detection task, especially their heuristic corner-matching algorithms. For example, CornerNet (Law and Deng 2018) determines corner pairs by local response similarity, which can cause severe confusion in detecting humans with similar appearances in the large spatial scale scene. CenterNet (Dual et al. 2019) predicts one more center point to filter out the false positives (FP), but it still can not perform well beyond applied to a gigapixel image, because the central regions of numerous FPs often cover the center point of a third person. Therefore, we may ask: Can we devise a robust corner matching algorithm for gigapixel-level full-body detection?

To answer the question and expand the applicability of corner-semantic-guided detectors for full-body detection on gigapixel-level images, we propose GigaHumanDet predicts two occupied corners of the bounding box, each of which is expressed explicitly and requires only two borders to be determined, improving the robustness in gigapixel crowds with various postures. To acquire discriminalize corner semantics for similar-looking persons, we devise an instance-guided learning strategy as shown in Figure 2. For reliably matching corners, we devise shape-aware bodyness which encodes the body shape embeddings at the corresponding corner location. To further purify the body shape embedding and make it more tolerant to the drastic scale variation, a Gaussian-inspired multi-precision regression strategy is devised to alleviate the difficulty and inaccuracy of once long-range regression. Note that the distance regression is decoupled from the corner prediction, so the corner pair can decode an accurate object box without being affected by the distance regression error. Equipped with robust bodyness, GigaHumanDet can reap promising performance by pairing corners with consistent body shapes.

Experimental results on gigapixel-level PANDA(Wang et al. 2020) benchmark show GigaHumanDet yields a new SOTA accuracy, in terms of 82.4% on AP_{50}, boosting 60.8% than CornerNet baseline and surpassing other methods by more than 10%. Further, the competitive results on STCrowd verify the applicability of our method to general pedestrian detection. Our contributions can be summarized as follows:

- This paper unleashes the power of corner modeling approach on gigapixel-level full-body detection, and we demonstrate that it is more suitable and robust than center-regression-guided methods for this task.
- We design instance-guided learning and multi-precision strategy to acquire discriminative corner semantics. We propose shape-aware bodyness to provide reliable corner-matching guidance for large-scale dense scenes.
- GigaHumanDet achieves the SOTA accuracy on the gigapixel level detection task and outperforms other advanced methods by 10%.

Related Work

Object Detection on High-Resolution Images

Object detection on large-scale HR images has become a challenging task. A gigapixel-level human-centric PANDA dataset(Wang et al. 2020) is published and its resolution has reached 25,000 $\times 14,000$. Due to wide FoV and high resolution, pedestrians have various postures as well as occlusions, and drastic scale changes exist, which degrades the accuracy of modern detectors developed on $\mathrm{COCO}(\mathrm{Lin}$ et al. 2014).

Center-Guided and Corner-Guided Methods

The center-guided detectors utilize centers and width/height to encode boxes. Most of them(He et al. 2017; Cai and Vasconcelos 2018; Ge et al. 2021) take the center as a reference point and regress object size. Different from the above methods, the corner-guided detector(Law and Deng 2018; Duan et al. 2019) is proposed to estimate corners and match them to compose the final box. But for gigapixel images, humans with similar appearances cause great confusion
when matching corners. Our GigaHumanDet employs the corner modeling method and tackles the matching problem by setting robust body-shape embedding for each corner.

Pedestrian Detection

The pedestrian detection task has been widely studied (Cai et al. 2016). Some full body detectors try to lift the accu-

Figure 7: Dynamic resolution of GOT for high-resolution images. In the dual-page paper reading mode shown in the figure (from [21]), the input resolution of the original GOT is not sufficient to handle it. Therefore, we adapt dynamic resolution technology to make the model no longer limited to the size of the image.

Prompt: OCR with format across multi pages:

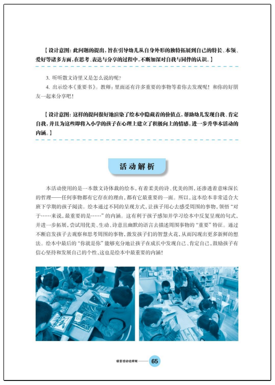

【设计意图：此问题的提出，旨在引导幼儿从自身外形的独特拓展到自己的特长、本领、爱好等诸多方面，在思考、表达与分享的过程中，不断加深对自我与同伴的认识。】

3．听听散文诗里又是怎么说的呢？

4．出示绘本《重要书》。教师：里面还有许多重要的事物等着你去发现呢！和你的好朋友一起来分享吧！

【设计意图：这样的提问很好地渲染了绘本中隐藏着的价值点，帮助幼儿发现自我、肯定自我，并且为这些即将入小学的孩子在心理上建立了积极向上的情感，进一步升华本活动的内涵。】

活动解析

本活动使用的是一本散文诗体裁的绘本，有着柔美的诗、优美的图，还渗透着意味深长的哲理——任何事物都有它存在的理由，都有它最重要的一面。所以，这本绘本非常适合大班下学期的孩子阅读。绘本通过不同的呈现方式，让孩子用心去感受周围的事物，领悟"对于……来说，最重要的是……"的内涵。这有利于孩子感知并学习绘本中反复呈现的句式，并进一步拓展，尝试用优美、生动、诗意且幽默的语言去描述周围事物的"重要"特征。通过不断启发孩子去观察和思考周围的事物，激发孩子们的智慧火花，从而闪现出更多新鲜的想法。绘本中最后的"你就是你"能够充分地让孩子在成长中发现自己、肯定自己，鼓励孩子有信心坚持和发展自己的个性，这也是绘本中最重要的内涵！

语言活动这样做——65

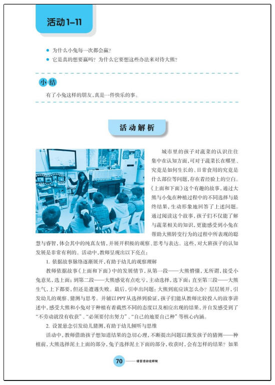

活动1–11

- 为什么小兔每一次都会赢？
- 它是真的想要赢吗？为什么它要想这些办法来对待大熊？

小结

有了小兔这样的朋友，真是一件快乐的事。

活动解析

城市里的孩子对蔬菜的认识往往集中在认知方面，可对于蔬菜长在哪里、究竟是如何生长的、日常食用的究竟是什么部位等问题，存在着经验上的空白。《上面和下面》这个有趣的故事，通过大熊与小兔在种植过程中的不同选择与最终结果，生动形象地回答了上述问题。通过阅读这个故事，孩子们不仅能了解与蔬菜相关的知识，更能感受到小兔在帮助大熊转变行为的过程中所表现的聪慧与睿智，体会其中的纯真友情，并展开积极的观察、思考与表达。这些，对大班孩子的认知发展是非常有利的。活动中，教师呈现出以下亮点：

1．依据故事脉络逐渐展开，有助于幼儿的观察理解

教师依据故事《上面和下面》中的发展情节，从第一段——大熊懵懂，无所谓，接受小兔意见，选上面；到第二段——大熊感觉有点吃亏，主动选择，选下面；直至第三段——大熊生气，上下都要，但还是遭遇失败。最后，引申出问题：大熊到底应该怎么办？层层展开，引发幼儿的观察、猜测与思考。并辅以PPT从选择到验证，孩子们能从教师比较投入的故事讲述中，感受大熊和小兔对于种植有着截然不同的态度以及相应出现的结果，并自发感受到了"不劳动就没有收获"、"必须要付出努力"、"自己的地要自己种"等核心内涵。

2．设置悬念引发幼儿猜测，有助于幼儿倾听与思维

活动中，教师借助孩子想知道结果的急切心理，不断提出问题以激发孩子的猜测——种植前，大熊选择泥土上面的部分，兔子选择泥土下面的部分，收获时，会有怎样的结果？如果

70——语言活动这样做

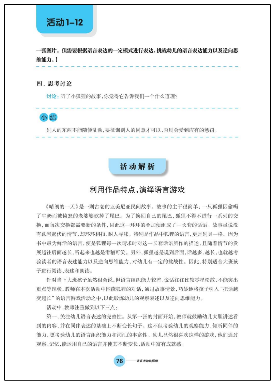

活动1–12

一张图片。但需要根据语言表达的一定模式进行表达，挑战幼儿的语言表达能力以及逆向思维能力。】

四、思考讨论

讨论：听了小狐狸的故事，你觉得它告诉我们一个什么道理？

小结

别人的东西不能随便乱动，要征询别人的同意才可以，否则会受到应有的惩罚。

活动解析

利用作品特点，演绎语言游戏

《晴朗的一天》是一则古老的亚美尼亚民间故事。故事的主干很简单：一只狐狸因偷喝了牛奶而被愤怒的老婆婆砍掉了尾巴。为了换回自己的尾巴，狐狸不得不进行一系列的交换，而每次交换都需要新的条件，因此这一环环的叠加便组成了一长套的话语。故事虽说没有跌宕起伏的情节，却环环相扣、耐人寻味。特别是作品中狐狸的语言，更是别具一格。因为书中最为鲜活的语言，便是狐狸每一次请求时对这一长套话语所作的描述，且随着情节的发展越往后面越长，听起来也越是滑稽可笑。另外，狐狸越是说到后面，话越多、越长，也就越考验读者的语言表述能力以及逆向思维能力，对幼儿有一定的挑战性。因此，特别适合大班孩子进行阅读、表述和朗读。

针对当下大班孩子虽然很会说，但语言组织能力较差、说话往往比较零星松散、不能突出重点等现状，教师在本次活动中围绕狐狸的对话，通过故事情景，巧妙地将孩子引入"把话越变越长"的语言游戏活动之中，以此锻炼幼儿的观察表述以及逆向思维能力。

活动中，教师注重做到以下三点：

第一，关注幼儿语言表述的完整性。从第一张的封面开始，教师就鼓励幼儿大胆讲述看到的内容，并在同伴表述的基础上不断变长句子。这不但考验幼儿的观察能力、倾听同伴的能力，更考验幼儿的语言组织能力和词汇的丰富性。幼儿显然很喜欢这样的游戏，他们通过观察、记忆，能运用自己的语言并使其不断变长，活动中富有成就感。

76——语言活动这样做

Output:

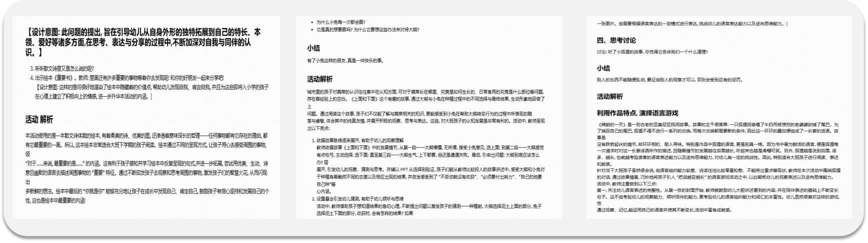

【设计意图: 此问题的提出, 旨在引导幼儿从自身外形的独特拓展到自己的特长、本领、爱好等诸多方面,在思考、表达与分享的过程中,不断加深对自我与同伴的认识。】

3. 听听散文诗里又是怎么说的呢?
4. 出示绘本《重要书》。教师: 里面还有许多重要的事物等着你去发现呢! 和你的好朋友一起来分享吧!
【设计意图: 这样的提问很好地渲染了绘本中隐藏着的价值点, 帮助幼儿发现自我、肯定自我, 并且为这些即将入小学的孩子在心理上建立了积极向上的情感, 进一步升华本活动的内涵。】

活动 解析

本活动使用的是一本散文诗体裁的绘本, 有着柔美的诗、优美的图, 还渗透着意味深长的哲理——任何事物都有它存在的理由, 都有它最重要的一面。所以, 这本绘本非常适合大班下学期的孩子阅读。绘本通过不同的呈现方式, 让孩子用心去感受周围的事物, 领
"对于......来说, 最重要的是......" 的内涵。这有利于孩子感知并学习绘本中反复呈现的句式,并进一步拓展, 尝试用优美、生动、诗意且幽默的语言去描述周围事物的 "重要" 特征。通过不断启发孩子去观察和思考周围的事物, 激发孩子们的智慧火花, 从而闪现出
多新鲜的想法。绘本中最后的 "你就是你" 能够充分地让孩子在成长中发现自己、肯定自己, 鼓励孩子有信心坚持和发展自己的个性, 这也是绘本中最重要的内涵!

- 为什么小兔每一次都会赢?
- 它是真的想要赢吗? 为什么它要想这些办法来对待大熊?

小结

有了小兔这样的朋友, 真是一件快乐的事。

活动解析

城市里的孩子对蔬菜的认识往往集中在认知方面, 可对于蔬菜长在哪里、究竟是如何生长的、日常食用的究竟是什么部位等问题, 存在着经验上的空白。《上面和下面》这个有趣的故事, 通过大熊与小兔在种植过程中的不同选择与最终结果, 生动形象地回答了上
问题。通过阅读这个故事, 孩子们不仅能了解与蔬菜相关的知识, 更能感受到小兔在帮助大熊转变行为的过程中所表现的聪慧与睿智, 体会其中的纯真友情, 并展开积极的观察、思考与表达。这些, 对大班孩子的认知发展是非常有利的。活动中, 教师呈现出以下亮点:

1. 依据故事脉络逐渐展开, 有助于幼儿的观察理解
   教师依据故事《上面和下面》中的发展情节, 从第一段——大熊懵懂, 无所谓, 接受小兔意见, 选上面; 到第二段——大熊感觉有点吃亏, 主动选择, 选下面; 直至第三段——大熊生气, 上下都要, 但还是遭遇失败。最后, 引申出问题: 大熊到底应该怎么办? 层
   展开, 引发幼儿的观察、猜测与思考。并辅以 PPT 从选择到验证, 孩子们能从教师比较投入的故事讲述中, 感受大熊和小兔对于种植有着截然不同的态度以及相应出现的结果, 并自发感受到了 "不劳动就没有收获"、"必须要付出努力"、"自己的地要自己种"等
   心内涵。
2. 设置悬念引发幼儿猜测, 有助于幼儿倾听与思维
   活动中, 教师借助孩子想知道结果的急切心理, 不断提出问题以激发孩子的猜测——种植前, 大熊选择泥土上面的部分, 兔子选择泥土下面的部分, 收获时, 会有怎样的结果? 如果

一张图片。但需要根据语言表达的一定模式进行表达, 挑战幼儿的语言表达能力以及逆向思维能力。]

四、思考讨论

讨论: 听了小狐狸的故事, 你觉得它告诉我们一个什么道理?

小结

别人的东西不能随便乱动, 要征询别人的同意才可以, 否则会受到应有的惩罚。

活动解析

利用作品特点, 演绎语言游戏

《晴朗的一天》是一则古老的亚美尼亚民间故事。故事的主干很简单: 一只狐狸因偷喝了牛奶而被愤怒的老婆婆砍掉了尾巴。为了换回自己的尾巴, 狐狸不得不进行一系列的交换, 而每次交换都需要新的条件, 因此这一环环的叠加便组成了一长套的话语。故事虽
没有跌宕起伏的情节, 却环环相扣、耐人寻味。特别是作品中狐狸的语言, 更是别具一格。因为书中最为鲜活的语言, 便是狐狸每一次请求时对这一长套话语所作的描述, 且随着情节的发展越往后面越长, 听起来也越是滑稽可笑。另外, 狐狸越是说到后面, 话多、越长, 也就越考验读者的语言表述能力以及逆向思维能力, 对幼儿有一定的挑战性。因此, 特别适合大班孩子进行阅读、表述和朗读。
针对当下大班孩子虽然很会说, 但语言组织能力较差、说话往往比较零星松散、不能突出重点等现状, 教师在本次活动中围绕狐狸的对话, 通过故事情景, 巧妙地将孩子引入 "把话越变越长" 的语言游戏活动之中, 以此锻炼幼儿的观察表述以及逆向思维能力。
活动中, 教师注重做到以下三点:
第一, 关注幼儿语言表述的完整性。从第一张的封面开始, 教师就鼓励幼儿大胆讲述看到的内容, 并在同伴表述的基础上不断变长句子。这不但考验幼儿的观察能力、倾听同伴的能力, 更考验幼儿的语言组织能力和词汇的丰富性。幼儿显然很喜欢这样的游戏, 他
通过观察、记忆,能运用自己的语言并使其不断变长,活动中富有成就感。

Figure 8: Multi-page (document) OCR ability of GOT. With this feature, researchers can continue to train the GOT with multi-page PDF-text pairs, such as Arxiv paper with *.tex* file.

Prompt: OCR with format: **Output:**

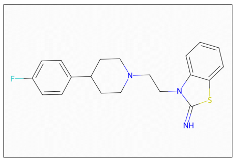

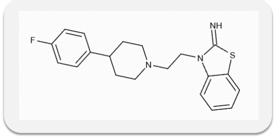

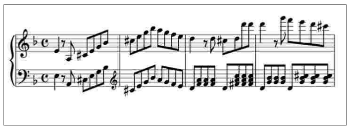

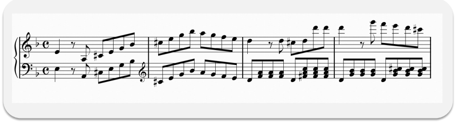

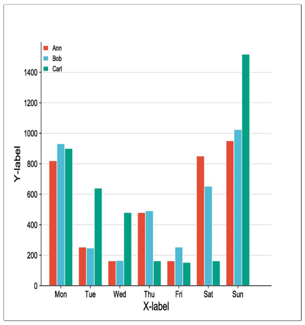

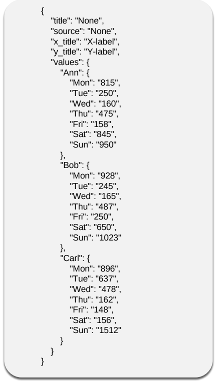

```
{
  "title": "None",
  "source": "None",
  "x_title": "X-label",
  "y_title": "Y-label",
  "values": {
    "Ann": {
      "Mon": "815",
      "Tue": "250",
      "Wed": "160",
      "Thu": "475",
      "Fri": "158",
      "Sat": "845",
      "Sun": "950"
    },
    "Bob": {
      "Mon": "928",
      "Tue": "245",
      "Wed": "165",
      "Thu": "487",
      "Fri": "250",
      "Sat": "650",
      "Sun": "1023"
    },
    "Carl": {
      "Mon": "896",
      "Tue": "637",
      "Wed": "478",
      "Thu": "162",
      "Fri": "148",
      "Sat": "156",
      "Sun": "1512"
    }
  }
}
```

Figure 9: More general OCR results. GOT can process molecular formulas, sheet music, and charts.

Prompt: OCR with format:

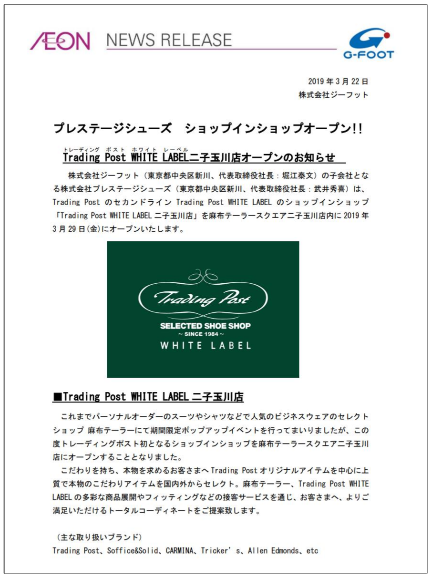

ÆON NEWS RELEASE G-FOOT

2019 年 3 月 22 日
株式会社ジーフット

プレステージシューズ　ショップインショップオープン!!

トレーディング　ポスト　ホワイト　レーベル
Trading Post WHITE LABEL二子玉川店オープンのお知らせ

株式会社ジーフット（東京都中央区新川、代表取締役社長：堀江泰文）の子会社となる株式会社プレステージシューズ（東京都中央区新川、代表取締役社長：武井秀喜）は、Trading Post のセカンドライン Trading Post WHITE LABEL のショップインショップ「Trading Post WHITE LABEL 二子玉川店」を麻布テーラースクエア二子玉川店内に 2019 年 3 月 29 日(金)にオープンいたします。

Trading Post
SELECTED SHOE SHOP
~ SINCE 1984 ~
WHITE LABEL

■Trading Post WHITE LABEL 二子玉川店

これまでパーソナルオーダーのスーツやシャツなどで人気のビジネスウェアのセレクトショップ 麻布テーラーにて期間限定ポップアップイベントを行ってまいりましたが、この度トレーディングポスト初となるショップインショップを麻布テーラースクエア二子玉川店にオープンすることとなりました。

こだわりを持ち、本物を求めるお客さまへ Trading Post オリジナルアイテムを中心に上質で本物のこだわりアイテムを国内外からセレクト。麻布テーラー、Trading Post WHITE LABEL の多彩な商品展開やフィッティングなどの接客サービスを通じ、お客さまへ、よりご満足いただけるトータルコーディネートをご提案致します。

（主な取り扱いブランド）
Trading Post、Soffice&Solid、CARMINA、Tricker’s、Allen Edmonds、etc

Output:

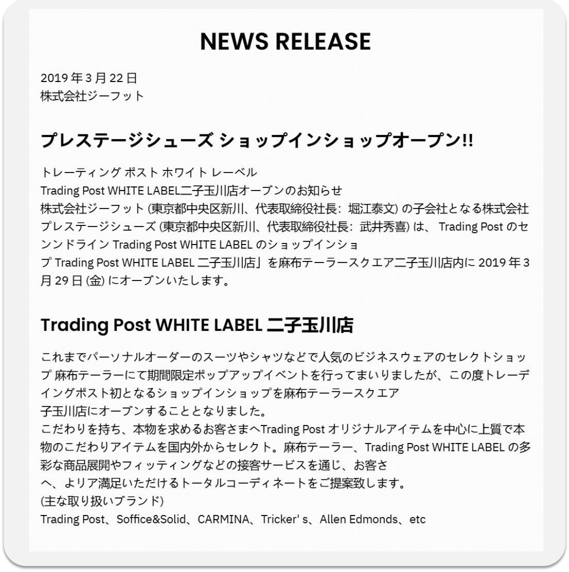

NEWS RELEASE

2019 年 3 月 22 日
株式会社ジーフット

プレステージシューズ ショップインショップオープン!!

トレーディング ポスト ホワイト レーベル
Trading Post WHITE LABEL二子玉川店オープンのお知らせ
株式会社ジーフット (東京都中央区新川、代表取締役社長: 堀江泰文) の子会社となる株式会社プレステージシューズ (東京都中央区新川、代表取締役社長: 武井秀喜) は、 Trading Post のセンドライン Trading Post WHITE LABEL のショップインショ
プ Trading Post WHITE LABEL 二子玉川店」を麻布テーラースクエア二子玉川店内に 2019 年 3 月 29 日 (金) にオープンいたします。

Trading Post WHITE LABEL 二子玉川店

これまでパーソナルオーダーのスーツやシャツなどで人気のビジネスウェアのセレクトショップ 麻布テーラーにて期間限定ポップアップイベントを行ってまいりましたが、この度トレーディングポスト初となるショップインショップを麻布テーラースクエア
子玉川店にオープンすることとなりました。
こだわりを持ち、本物を求めるお客さまへTrading Post オリジナルアイテムを中心に上質で本物のこだわりアイテムを国内外からセレクト。麻布テーラー、Trading Post WHITE LABEL の多彩な商品展開やフィッティングなどの接客サービスを通じ、お客さ
へ、よリア満足いただけるトータルコーディネートをご提案致します。
(主な取り扱いブランド)
Trading Post、Soffice&Solid、CARMINA、Tricker' s、Allen Edmonds、etc

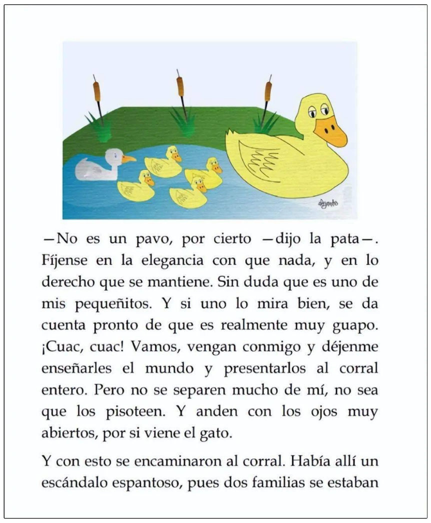

—No es un pavo, por cierto —dijo la pata—. Fíjense en la elegancia con que nada, y en lo derecho que se mantiene. Sin duda que es uno de mis pequeñitos. Y si uno lo mira bien, se da cuenta pronto de que es realmente muy guapo. ¡Cuac, cuac! Vamos, vengan conmigo y déjenme enseñarles el mundo y presentarlos al corral entero. Pero no se separen mucho de mí, no sea que los pisoteen. Y anden con los ojos muy abiertos, por si viene el gato.

Y con esto se encaminaron al corral. Había allí un escándalo espantoso, pues dos familias se estaban

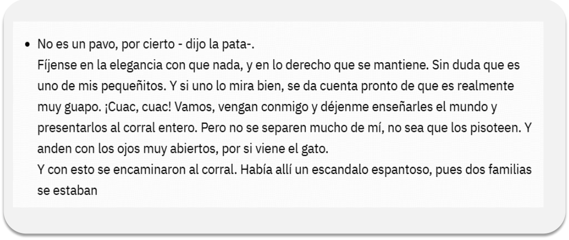

- No es un pavo, por cierto - dijo la pata-.
  Fíjense en la elegancia con que nada, y en lo derecho que se mantiene. Sin duda que es uno de mis pequeñitos. Y si uno lo mira bien, se da cuenta pronto de que es realmente muy guapo. ¡Cuac, cuac! Vamos, vengan conmigo y déjenme enseñarles el mundo y presentarlos al corral entero. Pero no se separen mucho de mí, no sea que los pisoteen. Y anden con los ojos muy abiertos, por si viene el gato.
  Y con esto se encaminaron al corral. Había allí un escandalo espantoso, pues dos familias se estaban

Figure 10: We do not specifically introduce additional OCR capabilities for GOT other than Chinese and English. Yet the PDF data we crawled may contain a small amount of text in other languages, leading to the GOT seeming to have the ability to recognize other languages. However, we cannot guarantee the OCR quality of other languages. Therefore, we recommend fine-tuning the model with corresponding data if this feature is needed.

References

[1] Casia-hwdb2-line. https://huggingface.co/datasets/Teklia/CASIA-HWDB2-line (2024) 6

[2] Iam-line. https://huggingface.co/datasets/Teklia/IAM-line (2024) 6

[3] Norhand-v3-line. https://huggingface.co/datasets/Teklia/NorHand-v3-line (2024) 6

[4] Bai, J., Bai, S., Chu, Y., Cui, Z., Dang, K., Deng, X., Fan, Y., Ge, W., Han, Y., Huang, F., Hui, B., Ji, L., Li, M., Lin, J., Lin, R., Liu, D., Liu, G., Lu, C., Lu, K., Ma, J., Men, R., Ren, X., Ren, X., Tan, C., Tan, S., Tu, J., Wang, P., Wang, S., Wang, W., Wu, S., Xu, B., Xu, J., Yang, A., Yang, H., Yang, J., Yang, S., Yao, Y., Yu, B., Yuan, H., Yuan, Z., Zhang, J., Zhang, X., Zhang, Y., Zhang, Z., Zhou, C., Zhou, J., Zhou, X., Zhu, T.: Qwen technical report. arXiv preprint arXiv:2309.16609 (2023) 6

[5] Bai, J., Bai, S., Yang, S., Wang, S., Tan, S., Wang, P., Lin, J., Zhou, C., Zhou, J.: Qwen-vl: A versatile vision-language model for understanding, localization, text reading, and beyond. arXiv preprint arXiv:2308.12966 (2023) 1, 4, 9, 10

[6] Blecher, L., Cucurull, G., Scialom, T., Stojnic, R.: Nougat: Neural optical understanding for academic documents. arXiv preprint arXiv:2308.13418 (2023) 4, 6, 8, 9

[7] Calvo-Zaragoza, J., Jr, J.H., Pacha, A.: Understanding optical music recognition. ACM Computing Surveys (CSUR) **53**(4), 1–35 (2020) 7

[8] Chen, J., Kong, L., Wei, H., Liu, C., Ge, Z., Zhao, L., Sun, J., Han, C., Zhang, X.: Onechart: Purify the chart structural extraction via one auxiliary token. arXiv preprint arXiv:2404.09987 (2024) 7, 10

[9] Chen, Z., Wang, W., Tian, H., Ye, S., Gao, Z., Cui, E., Tong, W., Hu, K., Luo, J., Ma, Z., et al.: How far are we to gpt-4v? closing the gap to commercial multimodal models with open-source suites. arXiv preprint arXiv:2404.16821 (2024) 1, 3, 4, 8, 9

[10] Du, Y., Li, C., Guo, R., Cui, C., Liu, W., Zhou, J., Lu, B., Yang, Y., Liu, Q., Hu, X., et al.: Pp-ocrv2: Bag of tricks for ultra lightweight ocr system. arXiv preprint arXiv:2109.03144 (2021) 1, 4, 5

[11] Graves, A., Fernández, S., Gomez, F., Schmidhuber, J.: Connectionist temporal classification: Labelling unsegmented sequence data with recurrent neural networks. In: International Conference on Machine Learning (ICML) (2006) 4

[12] Gu, J., Meng, X., Lu, G., Hou, L., Minzhe, N., Liang, X., Yao, L., Huang, R., Zhang, W., Jiang, X., et al.: Wukong: A 100 million large-scale chinese cross-modal pre-training benchmark. Advances in Neural Information Processing Systems **35**, 26418–26431 (2022) 5

[13] Hu, A., Xu, H., Ye, J., Yan, M., Zhang, L., Zhang, B., Li, C., Zhang, J., Jin, Q., Huang, F., et al.: mplug-docowl 1.5: Unified structure learning for ocr-free document understanding. arXiv preprint arXiv:2403.12895 (2024) 9, 10

[14] LeCun, Y., Bottou, L., Bengio, Y., Haffner, P.: Gradient-based learning applied to document recognition. Proceedings of the IEEE **86**(11), 2278–2324 (1998) 4

[15] Li, J., Li, D., Savarese, S., Hoi, S.: Blip-2: Bootstrapping language-image pre-training with frozen image encoders and large language models. arXiv preprint arXiv:2301.12597 (2023) 3

[16] Li, M., Lv, T., Chen, J., Cui, L., Lu, Y., Florencio, D., Zhang, C., Li, Z., Wei, F.: Trocr: Transformer-based optical character recognition with pre-trained models. In: Proceedings of the AAAI Conference on Artificial Intelligence. vol. 37, pp. 13094–13102 (2023) 4

[17] Li, Y., Mao, H., Girshick, R., He, K.: Exploring plain vision transformer backbones for object detection. In: European conference on computer vision. pp. 280–296. Springer (2022) 5

[18] Liao, M., Shi, B., Bai, X., Wang, C., Lu, T., Mei, T.: Textboxes: A fast text detector with a single deep neural network. In: Proceedings of the Thirty-First AAAI Conference on Artificial Intelligence (2017) 4

[19] Liao, M., Zou, Z., Wan, Z., Yao, C., Bai, X.: Real-time scene text detection with differentiable binarization and adaptive scale fusion. IEEE transactions on pattern analysis and machine intelligence **45**(1), 919–931 (2022) 4

[20] Liu, C., Wei, H., Chen, J., Kong, L., Ge, Z., Zhu, Z., Zhao, L., Sun, J., Han, C., Zhang, X.: Focus anywhere for fine-grained multi-page document understanding. arXiv preprint arXiv:2405.14295 (2024) 4, 8, 9, 10

[21] Liu, C., Wei, H., Yang, J., Liu, J., Li, W., Guo, Y., Fang, L.: Gigahumandet: Exploring full-body detection on gigapixel-level images. In: Proceedings of the AAAI Conference on Artificial Intelligence. vol. 38, pp. 10092–10100 (2024) 14

[22] Liu, F., Eisenschlos, J.M., Piccinno, F., Krichene, S., Pang, C., Lee, K., Joshi, M., Chen, W., Collier, N., Altun, Y.: Deplot: One-shot visual language reasoning by plot-to-table translation. In: Findings of the 61st Annual Meeting of the Association for Computational Linguistics (2023), https://arxiv.org/abs/2212.10505 10

[23] Liu, H., Li, C., Li, Y., Li, B., Zhang, Y., Shen, S., Lee, Y.J.: Llava-next: Improved reasoning, ocr, and world knowledge (January 2024), https://llava-vl.github.io/blog/2024-01-30-llava-next/ 3, 9

[24] Liu, H., Li, C., Wu, Q., Lee, Y.J.: Visual instruction tuning (2023) 1, 3, 4

[25] Liu, X., Zhang, R., Zhou, Y., Jiang, Q., Song, Q., Li, N., Zhou, K., Wang, L., Wang, D., Liao, M., et al.: Icdar 2019 robust reading challenge on reading chinese text on signboard. arXiv preprint arXiv:1912.09641 (2019) 8

[26] Liu, Y., Jin, L., Zhang, S., Luo, C., Zhang, S.: Curved scene text detection via transverse and longitudinal sequence connection. Pattern Recognition **90**, 337–345 (2019) 4

[27] Liu, Y., Yang, B., Liu, Q., Li, Z., Ma, Z., Zhang, S., Bai, X.: Textmonkey: An ocr-free large multimodal model for understanding document. arXiv preprint arXiv:2403.04473 (2024) 1, 3, 4, 9

[28] Loshchilov, I., Hutter, F.: Sgdr: Stochastic gradient descent with warm restarts. arXiv preprint arXiv:1608.03983 (2016) 8

[29] Loshchilov, I., Hutter, F.: Decoupled weight decay regularization. In: ICLR (2019) 8

[30] Lyu, P., Yao, C., Wu, W., Yan, S., Bai, X.: Multi-oriented scene text detection via corner localization and region segmentation. In: Proceedings of the IEEE conference on computer vision and pattern recognition. pp. 7553–7563 (2018) 4

[31] Masry, A., Kavehzadeh, P., Do, X.L., Hoque, E., Joty, S.: Unichart: A universal vision-language pretrained model for chart comprehension and reasoning. arXiv preprint arXiv:2305.14761 (2023) 10

[32] Masry, A., Long, D.X., Tan, J.Q., Joty, S., Hoque, E.: Chartqa: A benchmark for question answering about charts with visual and logical reasoning. arXiv preprint arXiv:2203.10244 (2022) 10

[33] Mathew, M., Karatzas, D., Jawahar, C.: Docvqa: A dataset for vqa on document images. In: Proceedings of the IEEE/CVF winter conference on applications of computer vision. pp. 2200–2209 (2021) 3

[34] Mertz, A., Slough, W.: Graphics with tikz. The PracTEX Journal **1**, 1–22 (2007) 7

[35] Methani, N., Ganguly, P., Khapra, M.M., Kumar, P.: Plotqa: Reasoning over scientific plots. In: Proceedings of the IEEE/CVF Winter Conference on Applications of Computer Vision. pp. 1527–1536 (2020) 10

[36] OpenAI: Gpt-4 technical report (2023) 1, 10

[37] Radford, A., Kim, J.W., Hallacy, C., Ramesh, A., Goh, G., Agarwal, S., Sastry, G., Askell, A., Mishkin, P., Clark, J., et al.: Learning transferable visual models from natural language supervision. In: International conference on machine learning. pp. 8748–8763. PMLR (2021) 1, 4

[38] Ríos-Vila, A., Calvo-Zaragoza, J., Paquet, T.: Sheet music transformer: End-to-end optical music recognition beyond monophonic transcription. arXiv preprint arXiv:2402.07596 (2024) 7

[39] Ríos-Vila, A., Rizo, D., Iñesta, J.M., Calvo-Zaragoza, J.: End-to-end optical music recognition for pianoform sheet music. International Journal on Document Analysis and Recognition (IJDAR) **26**(3), 347–362 (2023) 7

[40] Schuhmann, C., Beaumont, R., Vencu, R., Gordon, C., Wightman, R., Cherti, M., Coombes, T., Katta, A., Mullis, C., Wortsman, M., et al.: Laion-5b: An open large-scale dataset for training next generation image-text models. Advances in Neural Information Processing Systems **35**, 25278–25294 (2022) 5

[41] Shi, B., Yao, C., Liao, M., Yang, M., Xu, P., Cui, L., Belongie, S., Lu, S., Bai, X.: Icdar2017 competition on reading chinese text in the wild (rctw-17). In: 2017 14th iapr international conference on document analysis and recognition (ICDAR). vol. 1, pp. 1429–1434. IEEE (2017) 8

[42] Singh, A., Natarajan, V., Shah, M., Jiang, Y., Chen, X., Batra, D., Parikh, D., Rohrbach, M.: Towards vqa models that can read. In: Proceedings of the IEEE/CVF conference on computer vision and pattern recognition. pp. 8317–8326 (2019) 3

[43] Tian, Z., Huang, W., He, T., He, P., Qiao, Y.: Detecting text in natural image with connectionist text proposal network. In: European conference on computer vision. pp. 56–72. Springer (2016) 4

[44] Veit, A., Matera, T., Neumann, L., Matas, J., Belongie, S.: Coco-text: Dataset and benchmark for text detection and recognition in natural images. arXiv preprint arXiv:1601.07140 (2016) 8

[45] Wang, Y., Xie, H., Zha, Z.J., Xing, M., Fu, Z., Zhang, Y.: Contournet: Taking a further step toward accurate arbitrary-shaped scene text detection. In: Proceedings of the IEEE/CVF Conference on Computer Vision and Pattern Recognition. pp. 11753–11762 (2020) 4

[46] Wei, H., Kong, L., Chen, J., Zhao, L., Ge, Z., Yang, J., Sun, J., Han, C., Zhang, X.: Vary: Scaling up the vision vocabulary for large vision-language models. arXiv preprint arXiv:2312.06109 (2023) 1, 4, 5, 6, 9

[47] Wei, H., Kong, L., Chen, J., Zhao, L., Ge, Z., Yu, E., Sun, J., Han, C., Zhang, X.: Small language model meets with reinforced vision vocabulary. arXiv preprint arXiv:2401.12503 (2024) 6, 9

[48] Xia, R., Zhang, B., Ye, H., Yan, X., Liu, Q., Zhou, H., Chen, Z., Dou, M., Shi, B., Yan, J., Qiao, Y.: Chartx & chartvlm: A versatile benchmark and foundation model for complicated chart reasoning (2024) 10

[49] Ye, J., Hu, A., Xu, H., Ye, Q., Yan, M., Dan, Y., Zhao, C., Xu, G., Li, C., Tian, J., et al.: mplug-docowl: Modularized multimodal large language model for document understanding. arXiv preprint arXiv:2307.02499 (2023) 1, 3, 4

[50] Ye, J., Hu, A., Xu, H., Ye, Q., Yan, M., Xu, G., Li, C., Tian, J., Qian, Q., Zhang, J., et al.: Ureader: Universal ocr-free visually-situated language understanding with multimodal large language model. arXiv preprint arXiv:2310.05126 (2023) 3, 4, 9

[51] Zhang, C., Peng, G., Tao, Y., Fu, F., Jiang, W., Almpanidis, G., Chen, K.: Shopsign: A diverse scene text dataset of chinese shop signs in street views. arXiv preprint arXiv:1903.10412 (2019) 8

[52] Zhang, S.X., Zhu, X., Yang, C., Wang, H., Yin, X.C.: Adaptive boundary proposal network for arbitrary shape text detection. In: Proceedings of the IEEE/CVF International Conference on Computer Vision. pp. 1305–1314 (2021) 4

[53] Zhang, S., Roller, S., Goyal, N., Artetxe, M., Chen, M., Chen, S., Dewan, C., Diab, M., Li, X., Lin, X.V., et al.: Opt: Open pre-trained transformer language models. arXiv preprint arXiv:2205.01068 (2022) 5

[54] Zhong, X., Tang, J., Yepes, A.J.: Publaynet: largest dataset ever for document layout analysis. In: 2019 International conference on document analysis and recognition (ICDAR). pp. 1015–1022. IEEE (2019) 4

[55] Zhou, X., Yao, C., Wen, H., Wang, Y., Zhou, S., He, W., Liang, J.: East: An efficient and accurate scene text detector. In: Proceedings of the IEEE International Conference on Computer Vision (ICCV) (2017) 4